



Mohamed, A., Ardyani, T., Abu Bakar, S., Sagisaka, M., Umetsu, Y., Hamon, J. J., ... Eastoe, J. (2018). Rational design of aromatic surfactants for graphene/natural rubber latex nanocomposites with enhanced electrical conductivity. *Journal of Colloid and Interface Science*, 516, 34-47.  
<https://doi.org/10.1016/j.jcis.2018.01.041>

Peer reviewed version

License (if available):  
CC BY-NC-ND

Link to published version (if available):  
[10.1016/j.jcis.2018.01.041](https://doi.org/10.1016/j.jcis.2018.01.041)

[Link to publication record in Explore Bristol Research](#)  
PDF-document

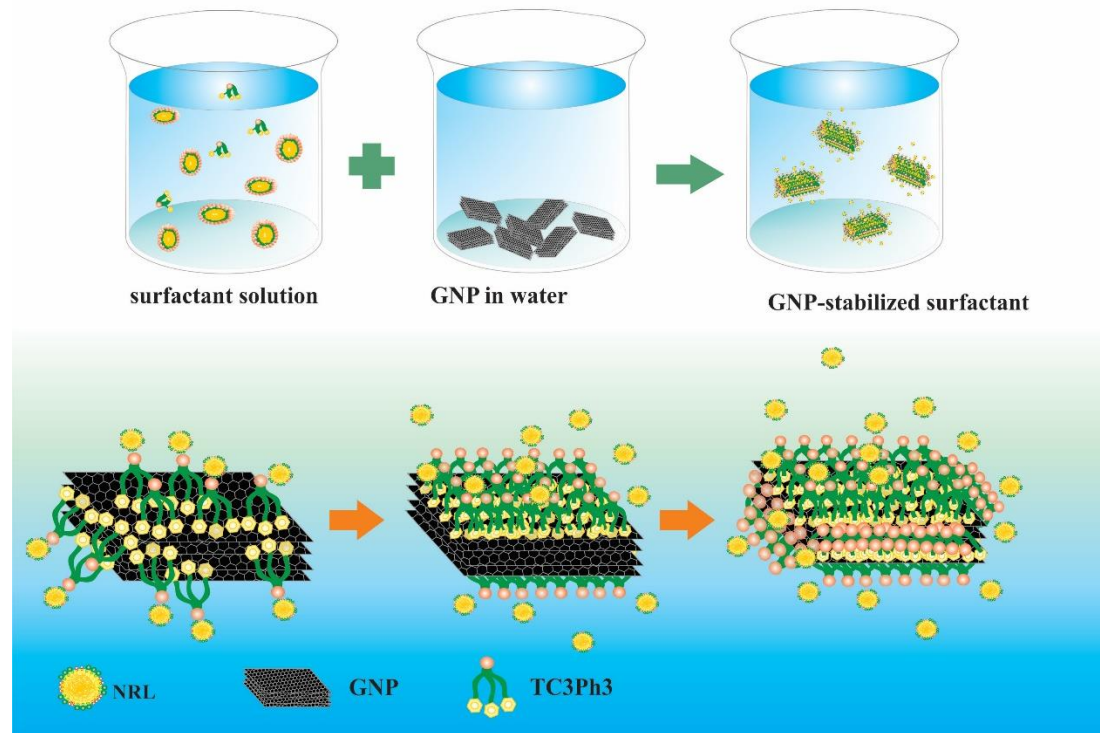
This is the author accepted manuscript (AAM). The final published version (version of record) is available online via Elsevier at <https://www.sciencedirect.com/science/article/pii/S002197971830050X?via%3Dihub> . Please refer to any applicable terms of use of the publisher.

## University of Bristol - Explore Bristol Research

### General rights

This document is made available in accordance with publisher policies. Please cite only the published version using the reference above. Full terms of use are available:  
<http://www.bristol.ac.uk/pure/about/ebr-terms>

## Graphical Abstract



AZMI – CHANGE THE ABBREVIATIONS IN THE lower part of Graphical abstract to read

Graphene nanoplatelets (GNPs), Natural rubber latex (NRL), Tri-chain anionic surfactant

[i.e. do not use these cryptic abbreviations such as TC3Ph3]

Rational Design of Aromatic Surfactants for Graphene/Natural Rubber Latex Nanocomposites  
with Enhanced Electrical Conductivity

Azmi Mohamed<sup>1,2\*</sup>, Tretya Ardyani<sup>1</sup>, Suriani Abu Bakar<sup>2</sup>, Masanobu Sagisaka<sup>3</sup>, Yasushi Umetsu<sup>3</sup>, J.J. Hamon<sup>4</sup>, Bazura Abdul Rahim<sup>5</sup>, Siti Rahmah Esa<sup>5</sup>, Abdul Khalil Shawkataly<sup>6</sup>, Mohamad Hafiz Mamat<sup>7</sup>, Stephen King<sup>8</sup>, Julian Eastoe<sup>9</sup>

<sup>1</sup>Department of Chemistry, <sup>2</sup>Nanotechnology Research Centre, Faculty of Science and Mathematics, Universiti Pendidikan Sultan Idris, 35900 Tanjong Malim, Perak, Malaysia

<sup>3</sup>Department of Frontier Materials Chemistry, Graduate School of Science and Technology, Hirosaki University, Bunkyo-cho 3, Hirosaki, Aomori 036-8561, Japan

<sup>4</sup>School of Chemistry, Monash University, Clayton 3800, Australia.

<sup>5</sup>MIMOS Semiconductor Sdn Bhd (MSSB), Technology Park Malaysia, 57000 Bukit Jalil, Kuala Lumpur,

<sup>6</sup>School of Industrial Technology, Universiti Sains Malaysia, 11700 Gelugor, Penang, Malaysia

<sup>7</sup>NANO-SciTech Centre (NST), Institute of Science (IOS), Universiti Teknologi MARA (UiTM), 40450 Shah Alam, Selangor, Malaysia

<sup>8</sup>Rutherford Appleton Laboratory, ISIS Spallation Source, Chilton, Oxfordshire, OX110QT, United Kingdom

<sup>9</sup>School of Chemistry, University of Bristol, Cantock's Close, Bristol, BS8 1TS, United Kingdom

\*Corresponding author. Tel.: +601548117582; fax: +601548117296

E-mail address: azmi.mohamed@fsmt.upsi.edu.my

### **Abstract**

Hypothesis: Graphene nanoplatelets (GNPs) can be dispersed in natural rubber matrices using surfactants. The stability and properties of these composites can be optimized by the choice of surfactants employed as stabilizers. Surfactants can be designed and synthesized to have enhanced compatibility with GNPs as compared to commercially available common surfactants. Including aromatic groups in the hydrophobic chain termini improves graphene compatibility of surfactants, which is expected to increase with the number of aromatic moieties per surfactant molecule. Hence, it is of interest to study the relationship between molecular structure, dispersion stability and electrical conductivity enhancement for single-, double-, and triple-chain anionic graphene-compatible surfactants.

Experiments: Graphene-philic surfactants, bearing two and three chains phenylated at their chain termini, were synthesized and characterized by proton nuclear magnetic resonance ( $^1\text{H}$  NMR) spectroscopy. These were used to formulate and stabilize dispersion of GNPs in natural rubber latex matrices, and the properties of systems comprising the new phenyl-surfactants were compared with commercially available surfactants, sodium dodecylsulfate (SDS) and sodium dodecylbenzenesulfonate (SDBS). Raman spectroscopy, field emission scanning electron microscopy (FESEM), atomic force microscopy (AFM), and high-resolution transmission electron microscopy (HRTEM) were used to study structural properties of the materials. Electrical conductivity measurements and Zeta potential measurements were used to assess the relationships

between surfactant architecture and nanocomposite properties. Small-angle neutron scattering (SANS) was used to study self-assembly structure of surfactants.

Findings: Of these different surfactants, the tri-chain aromatic surfactant TC3Ph3 (sodium 1,5-dioxo-1,5-bis(3-phenylpropoxy)-3-((3phenylpropoxy)carbonyl) pentane-2-sulfonate) was shown to be highly graphene-compatible (nanocomposite electrical conductivity =  $2.22 \times 10^{-5} \text{ S cm}^{-1}$ ), demonstrating enhanced electrical conductivity over nine orders of magnitude higher than neat natural rubber-latex matrix ( $1.51 \times 10^{-14} \text{ S cm}^{-1}$ ). Varying the number of aromatic moieties in the surfactants appears to cause significant differences to the final properties of the nanocomposites.

Keywords: Graphene nanoplatelets (GNPs), Natural rubber latex (NRL), Anionic surfactant, Surfactant stabilization, Surfactant self-assembly

List of abbreviations and symbols used:

$^1\text{H NMR}$	:	Proton nuclear magnetic resonance
AFM	:	Atomic force microscopy
CNTs	:	Carbon nanotubes
Cmc	:	Critical micelle concentration
DRC	:	Dry rubber content
FESEM	:	Field emission scanning electron microscopy
GNs	:	Graphene nanosheets
GNPs	:	Graphene nanoplatelets
HRTEM	:	High-resolution transmission electron microscopy
MWCNTs	:	Multi-walled carbon nanotubes
NR	:	Natural rubber
NRL	:	Natural rubber latex
PS	:	Polystyrene
PSS	:	Poly(sodium-4-styrenesulfonate)
SANS	:	Small-angle neutron scattering
SDBS	:	Sodium dodecylbenzenesulfonate
SDS	:	Sodium dodecylsulfate
SLD	:	Scattering-length density
TCE	:	Thermal conductivity enhancement
TSC	:	Total solid content
VOCs	:	Volatile organic compounds
$A_{\text{cmc}}$	:	Limiting headgroup areas at the cmc
$\gamma$	:	Surface tension
$\gamma_{\text{cmc}}$	:	Limiting surface tension at cmc
$I_{\text{D}}/I_{\text{G}}$	:	Intensity ratio of disorder-induced D-band and the G-band
$\Gamma$	:	Limiting surface excess
$\Gamma_{\text{m}}$	:	Limiting values of surface concentration of monolayers
$R_{\text{a}}$	:	Polar axis ratio of ellipsoidal micelle
$R_{\text{b}}$	:	Equatorial axis ratio of ellipsoidal micelle
$R_{\text{disk}}$	:	Stacked disk radius
$R_{\text{sphere}}$	:	Spherical micelle radius

$\theta$  : Surface coverages  
 $X$  : Aspect ratio of ellipsoidal micelle  
 $\zeta$ -potential : Zeta potential

## 1. Introduction

Over recent years there has been increased interest in the fundamental technological applications of graphene. Many labs are intensively exploring how to combine graphene with other materials, because doping even small amounts of graphene into host materials can have dramatic effects on physico-chemical properties. The wide range of potential applications of graphene call for an increased demand for graphene and derivatives, such as graphene nanoplatelets (GNPs). GNP is a multilayer graphene consisting of ~10-30 sheets of graphene with inherited monolayer graphene properties [1a,b]. As such, GNPs are much easier to obtain than graphene nanosheets (GNs) which have single-, bi- or few layers (no more than ten), and so have potential for large scale production of graphene-based materials [1a,b]. Now, the challenge is to explore which materials graphene can potentially add significant value.

For all its potential, graphene (whether single layer or multilayer) still suffers major drawbacks, especially in terms of stability when dispersed in solvents [2]. In this regard, it is obviously of importance to obtain graphene dispersions using low-cost and environmentally friendly techniques. Interest in aqueous graphene dispersions has been driven by the desire to minimize or eliminate VOCs (volatile organic compounds) in these formulations. One of the popular routes to prepare aqueous graphene dispersions is using surfactant-assisted sonication. Surfactant-stabilized graphene systems rely on repulsive inter-sheet interactions, provided by electrostatic or steric barriers, to overcome the natural destabilizing attractive inter-graphene interactions [3]. It is of special interest to formulate scalable graphene dispersions for practical for high volume manufacturing applications.

Natural rubber (NR) is a low cost and easy to obtain polymer with great potential for carbon-based polymer nanocomposites [4]. Despite the fact that NR is widely used for tire



manufacturing and in the medical applications, this hydrophilic polymer is generally less appropriate for electrical applications due to the absence of an internal conducting network. On the other hand, incorporating nanofillers such as graphene into NR matrices, is expected to generate electrically conductive nanocomposite materials. Therefore, over recent years, research on carbon nanomaterials and NR has been mainly dominated by development of enhanced electrically conductive nanocomposites [5, 6].

The advantages offered by surfactant-stabilized graphene dispersions, with the chemical anchoring offered by a hydrophilic NR matrix to fabricate nanocomposites, can be accomplished using a latex-based method to generate natural rubber latexes (NRLs). This technique was initially used for the dispersion of carbon nanotubes (CNTs) in polymer matrices [7, 8]. A key feature distinguishing this latex-based approach from other nanocomposite preparation methods (e.g. solvent mixing) is the use of surfactants. These added surfactants are physico-chemically adsorbed at graphene-polymer interfaces and reduce the surface energy (interfacial tension) by balancing lyophobic and lyophilic interactions. To date, there are only a limited number of studies concerning graphene/polymer nanocomposites obtained by this straightforward latex technique; and these report only commercially available surfactants, such as the anionic sodium dodecylsulfate (SDS), sodium dodecylbenzenesulfonate (SDBS) and the non-ionic Triton-X100 for example [9, 10]. Although these surfactants are said to offer improved graphene dispersion stability, undoubtedly certain optimal surfactant structures will offer greater graphene-compatibility, and surfactant concentration may also affect the efficiency of the nanofiller. Thus, when employing surfactants as dispersants for graphene, it is critical to select appropriate surfactant structures bearing “graphene-philic” moieties. For enhanced dispersion stability, the interaction between surfactants and graphenes must be strong enough to cover the graphene

surfaces with surfactant shells/layers which prevent close approach of the graphene sheets, and thereby prevent aggregation. It was hypothesized that surfactants bearing multiple aromatic moieties would lead to enhanced interactions with graphenes via  $\pi$ - $\pi$  interactions, and higher dispersion stabilities [11]. A recent paper showed that graphene compatibility can be enhanced by incorporating multiple aromatic groups, and also alkyl chain branching of the surfactants [9]. It is a logical step to suggest that increasing the number of aromatic rings in surfactant molecules could enhance further still graphene-surfactant dispersion stability.

Previously, a custom made aromatic analogue of the common anionic AOT surfactant has been reported to have very significant CNT-compatibility [5, 12]. Furthermore, introduction of a third surfactant chain TC3Ph3 (previously known as TCPh), being the tri-chain version of di-chain aromatic surfactant DC3Ph2 (known as DCPh) was shown to further enhance the dispersion stability. In that work, the synthesized surfactants were used to stabilize CNT dispersions in NRL to form conductive nanocomposites [5, 12]. Even though they are used at relatively low concentrations (0.016 – 0.032 M), in particular the tri-chain surfactant TC3Ph3, exhibited remarkable CNT-compatibility. Although there was only a small change in surfactant structure, a notably improved conductivity enhancement was observed (~2 orders of magnitude). This is markedly higher than found for the commercial surfactants SDS and SDBS when used under similar conditions. Clearly, these new custom-made CNT-compatible surfactants appear to have advantages over the common commercial surfactants used in major recent studies [7, 8, 10].

The purpose of this new paper is to investigate whether a similar strategy can be applied to obtain graphene-compatible surfactants. To reveal any specific effects using these custom made surfactants, comparisons of physico-chemical properties were also made with single chain commercial surfactants; SDS and SDBS (Table 1). The effect of surfactant concentration on

electrical conductivity enhancement of the resulting nanocomposites is also considered. The results show that the new DC3Ph2 and TC3Ph3 are viable surfactants for stabilizing dispersions of GNP in NRL matrices. These findings advance understanding of optimizing graphene-compatibility by modifying surfactant chain architecture. In particular, it is shown here that the number of aromatic moieties per surfactant molecule is an important parameter for improving properties of these nanocomposites.

## **2. Materials and methods**

### 2.1 Materials

The matrix polymer, NRL was supplied from the Malaysian Institute of Nuclear Technology Research, with the total solid content (TSC) and dry rubber content (DRC) being 54% and 56%, respectively. Methods to determine the TSC and DRC can be found elsewhere [13]. GNP powder (UG Pro 880, average thickness 0.98 – 3.54 nm) were obtained from UGENT Tech Pte Ltd and dried in an oven for 6h at 70°C prior to use. SDS (99%, System) and SDBS (technical grade, Sigma Aldrich) were used as received. The surfactants DC3Ph2 and TC3Ph3 were custom-made and synthesized as detailed previously [5]. Details regarding surfactant characterization can be found in **supplementary material**.

### 2.2 Preparation of Graphene Dispersion

The GNP dispersions were prepared using surfactants, and a Branson 5510 sonicator, with 135W of 42 kHz ultrasound. Surfactant concentrations were varied from 0 to 0.032 M. For comparable studies, the filler loading was fixed at 2 wt%, relative to the TSC of the NRL. A known amount of

GNP was initially dispersed in a 10 mL surfactant solution and stirred for 1 h. The resulting dispersions were then subjected to sonication for 2 h.

Here, the amount of filler in the composite was calculated based on the dry mass of NRL (TSC). For instance, to prepare composites starting from 2.5 g of NRL, we consider 1.35 g of dry rubber (solid content of 54%). Therefore, the amount of filler added to the surfactant solutions correspond to 2 wt% of 1.35 g dry rubber, giving the amount of 27.0 mg GNP powder.

### 2.3 Nanocomposite Preparation

The NRL (2.5 g) was subsequently added to the 10mL graphene-stabilized surfactant dispersions and stirred for 1 h. The mixtures were then sonicated (Branson 5510 sonicator) for 2 h and cast into a mould. Nanocomposites were obtained after drying in an oven at 70°C overnight.

### 2.4 Electrical conductivity measurements

Electrical conductivities of the nanocomposites were determined using a standard four-point probe method. All samples were cut into 15 mm x 15 mm and measured for the surface (in-plane) direction. For each sample, conductivity data represent the averages of three consecutive measurements. All conductivity measurements were performed at room temperature (25°C) with a programmable Keithley 2636A electrometer.

### 2.5 Characterization of Morphology

A variety of experimental tools were used to characterize the morphology of GNP dispersions and the subsequent GNP/NRL nanocomposites. The dispersion of GNP flakes in the NRL matrix was studied using Raman spectroscopy, field emission scanning electron microscopy (FESEM), atomic

force microscopy (AFM), and high-resolution transmission electron microscopy (HRTEM). To avoid charging the nanocomposites were coated with platinum (Pt) prior to SEM (Hitachi SU8020) imaging. To visualize the embedded microstructure of nanocomposites using HRTEM (JEOL 2100F), the samples were ultramicrotomed with a diamond knife to give sections with nominal thickness  $\sim 80$  nm. Raman spectroscopy was used to evaluate the graphitic structure of GNPs. The Raman spectra were collected using a Renishaw InVia micro Raman system spectrophotometer with a 514 nm argon-ion laser source. Five regions were measured for each nanocomposite. AFM imaging was performed using a JPK Nanowizard III in tapping mode. The cantilever used was antimony-doped silicon with a nominal force constant of 50 N/m and a resonant frequency 353 kHz (HQ:NSC 15/AL BS from MikroMasch). Imaging was performed using a line rate of 0.8 Hz, an integral gain between 10 and 50 Hz, a proportional gain of 0.001 Hz, and a drive amplitude of 0.025 V. All imaging was performed in air and approximately 20 degrees C.

## 2.6 Zeta Potential Measurements

Zeta potential measurements were performed by ELSZ-1000 Zeta-potential and Particle size Analyzer (Photal OTSUKA ELECTRONICS) with Smoluchowski equation as zeta potential conversion equation and 1 peak Lorentz fitting. Measurements were carried out with a flow cell at sampling time 400  $\mu$ s, cumulative number 7, measuring angle 15°, temperature 25 °C, pin hole size 50  $\mu$ m, cell constant 70.000  $\text{cm}^{-1}$ . Properties of aqueous mixtures (refractive index 1.3328, viscosity 0.8878 cP, and permittivity 78.3  $\text{Fm}^{-1}$ ) were used for calculation of zeta potential. Zeta potential values were finally obtained as average values of 10 runs for each sample.

## 2.7 Small-angle Neutron Scattering (SANS)

Small-Angle Neutron Scattering (SANS) studies were carried out on the time-of-flight LOQ instrument at ISIS, UK. The accessible Q range was  $0.007 - 0.23 \text{ \AA}^{-1}$ , arising from incident neutron wavelengths of  $\lambda = 2.2 - 10 \text{ \AA}$ . Absolute intensities for  $I(Q)$  ( $\text{cm}^{-1}$ ) were determined to within 5% by measuring the scattering from a partially deuterated polymer standard. Neutrons are scattered by short-range interactions with sample nuclei, the ‘scattering power’ of different components being defined by a scattering-length density (SLD),  $\rho$  ( $\text{cm}^{-2}$ ). The samples were prepared in 2 mm path-length quartz cells and held in a thermostatted automatic sample changer at  $25^\circ\text{C}$ . Data have been fitted using the SASView interactive fitting program, fixing scattering length density differences as calculated and fitting for micellar volume fraction and appropriate structural parameters as required by the different scattering laws (see **supplementary material**).

## 3. Results and discussion

### 3.1 Electrical conductivity of GNP/NRL composites

The development of latex technology as an economically scalable method to achieve uniform graphene dispersions has largely benefited from the extensive studies done with CNT/polymer nanocomposites [7, 8, 14]. Most studies have relied on improved physical properties of the nanocomposites to demonstrate how well the graphene is dispersed in the polymer matrices [1, 15]. In the development of semi-conductive polymer nanocomposites the aims are usually a low percolation threshold with significant enhancement value [16, 17]. For nanocomposites with insulating matrices to become electrically conductive, the filler concentration of must exceed the percolation threshold, where at certain loading fraction a system-spanning conductive network of

filler particles is formed, leading to an abrupt rise in electrical conductivity [18]. Interestingly, latex-based filler-polymer composites are usually expected to have lower percolation thresholds than similar composites prepared using either solvent mixing or melt blending [17, 19, 20].

A convenient way to convey the ability of each graphene-philic surfactant for dispersing GNPs into the NRL matrix is at a fixed graphene loading fraction, thereby facilitating direct comparison of the overall nanocomposite electrical conductivities. Here, conductivity is studied in terms of surfactant concentration with fixed GNP loading fraction (Figure 1, Table 2). The percolation test was conducted using SDBS surfactant, giving a value at 0.2 – 0.6 wt% for this standard system. This value is in a similar range with the extensive data collected for various surfactants using latex dispersion technology [9], and also the solvent mixing route [17, 21].

Without surfactant stabilizers, when dispersed in a NRL matrix ( $1.51 \times 10^{-14} \text{ S cm}^{-1}$ ), GNPs enhanced the electrical properties  $\sim 2$  orders of magnitude, giving an overall conductivity of  $3.56 \times 10^{-12} \text{ S cm}^{-1}$ . The widely used surfactant, SDS (0.032 M), indeed leads to a notable increase in electrical conductivity to  $1.76 \times 10^{-8} \text{ S cm}^{-1}$ . As evidenced by Fig. 1, changing to SDBS – which may be considered as SDS with one aromatic ring near to the headgroup, offers approximately an increase of 2 orders of magnitude in electrical conductivity over equivalent systems stabilized with SDS. The results and trends show a good agreement with previous work using multi-walled carbon nanotubes (MWCNTs) [5]. The double chain DC3Ph2 (previously known as AOTPh [5]) moderately increases the nanocomposite electrical conductivity up to  $9.36 \times 10^{-6} \text{ S cm}^{-1}$ . Further modification of the surfactant chain to be tri-chain surfactant TC3Ph3 (previously known as TCPH [5]) raised the electrical conductivity to  $2.22 \times 10^{-5} \text{ S cm}^{-1}$  at 0.016 M surfactant concentration. Attempts to increase the surfactant concentration (0.020 – 0.032 M) to disperse greater quantities of graphene in NRL matrix did not result in higher electrical conductivities of the nanocomposites.

Recent work by Wang et al. reported that graphene exfoliation increased with ionic surfactant concentration [24]. It was further stated that the graphene concentration decreased after reaching an optimum surfactant concentration. The phenomenon was explained using DLVO theory, that for a given interparticle separation higher surfactant concentration will act to lower the potential barrier experienced between neighboring graphene sheets, leading to aggregation. Interestingly, the results presented here support this: there is a maximum concentration for each surfactant to produce nanocomposites with optimum electrical conductivity.

In the field of thermal interfacial materials, the efficiency of any filler is characterized by its thermal conductivity enhancement (TCE), which is calculated on the basis of the thermal conductivity of the composite compared to the thermal conductivity of the pure polymer matrix [25]. A similar concept is applied here to quantify the surfactant and/or filler as well as dispersion technique efficiency. The electrical conductivity enhancement can be defined as;

$$\text{Enhancement} = \frac{\text{conductivity of nanocomposite}}{\text{conductivity of polymer}} \quad (\text{Eq 1})$$

Fig. 2 shows the conductivity enhancement of graphene/polymer nanocomposites using various techniques and nanofiller loadings (wt%). It can be seen that there is remarkable enhancement with the new nanocomposites introduced here at ~ 2wt% loading fraction, especially for TC3Ph3 surfactant. Although the enhancement is not as high as graphene-polystyrene (PS) stabilized by poly(sodium-4-styrenesulfonate) (PSS) surfactant [26, 27], TC3Ph3 is certainly more efficient since PSS was used at very high levels (~ 10-fold excess). Moreover, it can be seen that nanocomposites prepared using latex technology offer greater electrical conductivity enhancement than those made via solution mixing and polymerization [6, 21, 26, 28, 29]. Clearly, these recently developed surfactants appear to have some advantages over the PSS mentioned above, given the



ability to stabilize dispersions at lower levels, thus giving greater effective enhancements, and being water-based systems, they are certainly more economical and environmentally friendly. Previous studies focused on the final conductivity of the nanocomposites [17, 26, 27, 30], whereas the electrical conductivity enhancement value, which is one of the most simple ways to assess the dispersant and/or filler efficiency, has only received attention from a few groups.

The results above strongly point to the influence of extra surfactant chains on the graphene-compatibility, and also the number of aromatic rings per surfactant molecule. This has been hinted at by others in previous literature; that the presence and number of aromatic rings per stabilizer molecule will strengthen  $\pi$ - $\pi$  interactions between graphenes and surfactants [31-35]. Clearly, the surfactant chain structure and especially the extent of aromatic character are important factors for graphene-compatibility.

### 3.2 Incorporation of GNP in the NRL: Morphology

FESEM images give insight into the dispersion state of nanofillers inside the polymer matrix. Fig. 3 shows FESEM images of GNP (a and a') and NRL (b and b'). The image of exfoliated GNPs inside the polymer matrix is distinguishable by the appearance of bright flakes against a dark polymer matrix. As can be seen, the GNPs are present as flakes of different size and shapes, whereas the NRL appears as dark regions. The nature of such contrast can be explained by different secondary electrons generated in GNP and NRL, as explained elsewhere [8, 30].

Without surfactant, aggregated structures of GNP in the NRL matrix are observed, as indicated by the diamond arrows ( $\blacklozenge$ ). The agglomerated GNP structure appears as bulk pieces of filler at higher magnification instead of platelets (c') [30]. After introducing SDS and SDBS, the GNP aggregation seems to slightly decrease, giving more separated individual GNP flakes –

represented by the stealth arrow ( $\rightarrow$ ). Notably, the dispersion and stabilization of GNPs was notably increased with the aromatic surfactants DC3Ph2 and TC3Ph3, and it is even possible to see the presence of individual GNP flakes at higher magnification (f' and g'). Recalling the electrical conductivity measurements, it becomes apparent that there is a correlation between the extent of GNP dispersion and electrical properties of the nanocomposites. This again emphasizes the importance of designing and selecting optimized “graphene-philic” surfactants as stabilizers.

One of clearest ways to further characterize the morphology of nanofillers inside NRL matrices is with high resolution transmission electron microscopy (HRTEM). Fig. 4 (a-c) shows representative micrographs of ultramicrotomed thin section nanocomposites stabilized by the triple-chained TC3Ph3 surfactant. TEM micrographs reveal the presence of GNP particles as multilayer graphene sheets (Fig. 4a). Despite not achieving a high degree of exfoliation as compared to other studies [36, 37], the treatments with surfactant facilitate good dispersion of GNPs into the NRL matrix. The surfactant layers are thought to act as barriers between nearby GNPs from stacking as tactoids. It is important to mention that the GNPs are adhering to the latex particles (see Fig. 4b-c). The results suggest that TC3Ph3 surfactant provides good “bridging” between those two incompatible materials, GNPs and latex particles: this has also been found with other systems [6, 38].

The prepared nanocomposites were also characterized by AFM, which is widely used to complement other microscopic techniques used to characterize composite materials [1, 39, 40]. AFM allows for easy sample preparation and the natural samples can be studied, since neither conductive coatings nor staining are required [39, 40]. AFM tapping mode was chosen as the most appropriate imaging method to prevent damage to the probe or sample during imaging of the

surface. (Interested readers can refer to appropriate literature [40]). Representative AFM images of GNP/TC3Ph3/NRL in tapping mode are shown in Fig. 5.

The GNP surface height image (Fig. 5a) shows a textured surface, but otherwise no indication of a dispersed material. The oscillatory noise present throughout is thought to be caused by feedback in the system due to the elastic response of the surface; however, despite this, the phase image (Fig. 5b) clearly shows thoroughly dispersed components throughout in the NRL. Therefore, the enhanced electrical properties can be considered to have arisen from the interfacial interactions of GNP nanoparticles in the NRL.

Raman spectroscopy is a commonly used tool for the characterization of carbon materials since Raman scattering is strongly sensitive to the electronic structure of samples, and can give information about defects disorder, optical energy gaps, number of graphene layers, edge structure, amongst other properties [41, 42]. Figure 6 shows typical Raman spectra of GNPs with the characteristic peaks of graphite, namely the disorder band (D band) at  $\sim 1353 \text{ cm}^{-1}$  and the in-phase vibration of the graphite lattice (G band) at  $\sim 1580 \text{ cm}^{-1}$ . It is obvious that after dispersing GNP using surfactant, the D band and G band are only slightly shifted, being at  $\sim 1353 - 1358 \text{ cm}^{-1}$  and  $\sim 1581 \text{ cm}^{-1}$ , respectively.

Quantifying disorder in the GNPs was also attempted by analyzing the intensity ratio between the disorder-induced D-band and the G-band ( $I_D/I_G$ ). Comparing with the GNPs, it can be seen that the  $I_D/I_G$  ratios for the nanocomposites were markedly similar. A universal observation is that both the G and D bands do not undergo significant changes after surfactant treatment, indicating that the  $sp^2$  network remains essentially intact. Raman spectra described above agree well with a previous study using MWCNTs, indicating that the non-covalent functionalization of graphene sheets by the synthesized surfactants was successful [5, 12].

### 3.3 Surfactant stabilization: relationship between number of aromatic groups and dispersion stability – zeta potentials and molecular interactions

In charged colloidal systems, and with ionic surfactants as stabilizers, repulsive surface interactions are related to zeta ( $\zeta$ )-potential i.e. the electrical potential of the Stern layer [43-46]. Repulsive charge surface interactions are the underlying reasons for the successful dispersion of graphene using various types of surfactant [3, 47-49]. In such surface-charge stabilized colloidal systems zeta potential measurements are useful to gain information about the origin of dispersion stability.

A range of surfactants have been investigated as stabilizers, and it was found the zeta potential varied with surfactant chemical structure/type. For each sample, ten separate measurements were performed here, since previous work by Hassan et al. suggested that at least six separate measurements should be performed to ensure reproducibility [50]. As a general guide, when  $\zeta$ -potential lies at 0-10 mV the system will be unstable, 10 – 30 mV considered as moderately stable, 30 – 60 mV has a good stability while over 60 mV will give an excellent stability [45, 46]. Table 3 compares of electrical surface effects provided by surfactants used in this study. We observed  $\zeta$ -potential for graphene dispersions stabilized by SDS and SDBS respectively are -43 mV and -40 mV, which is well beyond the accepted value for colloidal stability. The results here are in line with the range of literature values for SDS and SDBS-stabilized graphene dispersions [3, 48].

Comparing the results for these two surfactants, it can be seen that the presence of one aromatic ring with SDBS has only a weak impact on  $\zeta$ -potential and colloid stabilization, considering that both are in similar range within experimental uncertainty. Moving to DC3Ph2 as dispersing agent gave rise to a notable increase in  $\zeta$ -potential to -69 mV. Among the surfactants

studied, TC3Ph3 resulted in a significant increase in  $\zeta$ -potential to reach -95 mV, thereby conferring high dispersion stability. This increased dispersion ability may explain the origin of the significant enhancement in electrical conductivity caused by the TC3Ph3 surfactant.

Examining the effects of surfactant types on  $\zeta$ -potential an interesting pattern emerges: higher  $\zeta$ -potentials were observed on increasing the number of aromatic moieties in the surfactant molecules. (However, from the aliphatic SDS to the aromatic SDBS the effect remains subtle). Work on adsorption of aromatic compounds using CNTs previously suggested that  $\pi$ - $\pi$  interactions between compounds and CNT-surfaces depend on the number, size and shape of the aromatic groups [11, 31].

Theoretical studies have identified that non-covalent interactions for  $\pi$ - $\pi$  systems with aromatic-bearing compounds may be rather complex, and may result from a combination of electrostatic, hydrophobic, and van der Waals interactions [51, 52]. Drawing parallels with those theoretical studies, stronger electrostatic interactions will also contribute to enhanced  $\pi$ - $\pi$  interactions by improving the stability of graphene-coated surfactant complexes. This trend may be explained by stronger hydrophobic interactions between the surfactants and graphene surfaces, as corroborated by the variations of aqueous surfactant properties shown in Table 1. As can be seen the cmc (which is one measure of overall surfactant “hydrophobicity”) in general decreases with increasing surfactant aromatic content. This trend with increasing the number of aromatic rings mirrors the changes in stability and properties of the GNP-latex systems discussed above.

### 3.4 Surfactant Self-Assembly: A SANS Study

Although visualization of the structure and nature of the GNP dispersions can be carried out using microscopy techniques e.g. AFM, TEM, SEM; these methods are not able to give reliable

information on about how the surfactants organize on GNPs. Despite that surfactant dispersions of graphene-based materials are of great interest, a clear picture of surfactant aggregation/adsorption remains limited. Simulation work has offered insight into how some commercial surfactants aggregate on the graphene surfaces, but many aspects still remain to be understood [53, 54]. Experimentally, small-angle neutron scattering (SANS) can provide useful information on the self-assembly structure surfactants with graphenes [55]. In the absence of inter-micellar interactions the scattering intensity  $I(Q)$  is proportional to the form factor,  $P(Q)$ , which reports information on particle size and shape. Full details of the scattering form factors and parameters of the models used in this study can be found in the **supplementary material**.

SANS profiles of solutions for aromatic surfactants are shown in Fig. 7 (SDS is not included). For direct comparisons, measurements were conducted at the same surfactant concentration and temperature. The scattering profiles for the surfactant solutions were fitted to form factors describing either a charged spherical or a charged ellipsoidal particle model, with a charge repulsion  $S(Q)$  structure factor peak following the Hayter-Penfold model [56]. Here, the scattering profiles of the SDBS solution was consistent with charged spherical micelles and a micellar radius ( $R_{\text{sphere}}$ ) of 22.0 Å (Table 4). The fitted micellar dimensions are  $R_{\text{sphere}} = 22.0$  Å (Table 4). At odds with the large number of SANS studies on SDS, SDBS has not been much explored. In an earlier study, Zhou et al. reported the formation of spherical micelle for various SDBS concentrations although they did not calculate the micellar radius [57]. The work presented here is in broad agreement with that of Cheng and Gulari which reported the formation of sphero-cylinder micelles with a radius of  $\sim 22$  Å [58]. A simulation study by Palazzesi et al. also predicted a spherical-ellipsoidal formation for SDBS with a mean micellar radius of 20 Å [59].

Moving to other surfactant structure, both of the di-chain and tri-chain compound; DC3Ph2 and TC3Ph3 scattering profiles were found to be well represented by charged ellipsoidal micelles and a  $P(Q)$  with polar axis ratio  $R_a$ , equatorial axis ratio  $R_b$  and aspect ratio  $X$  multiplied by an electrostatic repulsive  $S(Q)$  (Hayter-Penfold model) [56]. An overview of the parameters obtained using the model is given in Table 4. The work presented here is in agreement to that found in the literature, reporting micelle formation for the di-chain surfactant (AOT) and highly-branched tri-chain surfactant (TC14 surfactant) [60, 61]. The addition of the third surfactant chain would possibly make hydrocarbon chains expanded from the micellar center, forcing ellipsoidal micelles to fatten somewhat due to the extra phenyl rings. The equatorial dimension as seen by SANS thus increases by 8 Å.

Parallel SANS experiments with GNP dispersion were conducted and compared to those with the GNP-free surfactant solutions. A GNP dispersion in water without surfactant was also studied, showing no SANS and hence no evidence of colloidal structure/dispersion. When GNPs were dispersed with SDBS, the SANS data were still similar, analyses showing no significant changes in shape and size ( $R_{\text{sphere}} = 22.0 \text{ Å}$ ). The scattering intensities throughout the  $Q$ -range are slightly lower than those from the SDBS system, suggesting adsorption of SDBS on GNPs. This SANS behavior is analogous to the previous work on surfactant stabilization on CNT dispersions which is known to exhibit low  $Q$  scattering after surfactant adsorption [62-64]. Thus, the scattering from these spherical micelles is essentially unaffected, and indicates little perturbation to the spherical micelles of SDBS by GNP, suggesting weak graphene-SDBS interactions.

For GNP dispersed with DC3Ph2, aside from the intensity differences over  $Q < 0.03 \text{ Å}^{-1}$ , the scattering is still similar to the native DC3Ph2 solution, as was found with SDBS systems. The data set could be adequately fitted to a charged ellipsoidal form factor model multiplied by the

Hayter-Penfold  $S(Q)$  (fit parameters in Table 4). Interestingly, the micellar radii undergo significant changes with the polar radius being 20 Å larger, and the equatorial radius shrinking for the GNP dispersion. These differences can be attributed to the presence of GNPs dispersed in the DC3Ph2 micelles. It is clear that GNP dispersions are present, but beyond that the results cannot be further interpreted.

Introduction of GNP in the TC3Ph3 solution resulted higher SANS intensities, very different from those from the pure TC3Ph3 solution. Looking at the data on a logarithmic scale,  $I(Q)$  scales approximately as  $Q^{-2}$ , which is characteristic of 2-dimensional structures [55, 65, 66], and the fitted disk radius ( $R_{\text{disk}}$ ) is 286 Å. These general observations are distinctly different from those for the single- and di-chain surfactants, and in the case of TC3Ph3 the aggregate structure changes from ellipsoidal micelles to tactoid-type for the GNP dispersions. The SANS for GNP/TC3Ph3 and GNP/DC3Ph2 dispersions at different surfactant concentrations were also studied, and are given in **supplementary material** together with the fitted curves and parameters.

It is well known that surfactants form various aggregate morphologies in the presence of carbon nanomaterials [9, 10, 53, 54, 67]. However, the impact to the shape and size of aggregates are less studied and understood. On varying the number of surfactant chains (tails), it appears that the micelle shape and size transformation becomes pronounced. Further points of interest are the ellipsoid-to-disk transition of the tri-chain surfactants, and its relationship to the effectiveness in dispersing GNPs: these will be further discussed in the next section.

### 3.5 Model for Surfactant – Graphene Interactions

It is interesting to speculate on the plausible reasons for the observed micellar shape changes. Early studies on surfactant-aided CNT dispersions generated by ultrasound recognized the adsorption of



hydrophobic surfactant tails on CNT surfaces [10, 67]. The interactions between surfactant tails and CNT surfaces (or here graphene sheets) are therefore likely to be hydrophobic rather than Coulombic. Consequently, the affinity of surfactants for carbon surfaces is believed increase with the number of surfactant tails per molecule [5, 9].

In the current study, it is seen that the tri-chain surfactant TC3Ph3 does not behave like the other surfactants. A model is proposed (see Fig. 8) where the surfactant molecules interact with aromatic containing tails face-on, covering the graphene surfaces due to  $\pi$ - $\pi$  interactions. This organization will maximize the “tail-to-graphene” interactions and consequently minimize the contact of water molecules with graphene surfaces that would lead to destabilization [53, 67]. The hydrophilic surfactant parts will then arrange themselves facing away from the graphene surfaces and interact with the shell layer latex particles [68, 69].

Furthermore, experimental evidence shows that there is an ellipsoid micelle-to-stacked disk transition for the GNP-stabilized TC3Ph3 system. Rather than GNPs being dispersed by micelles, the surfactant molecules might preferentially adsorb on graphene surfaces. This seems likely, given that GNPs were shown previously to be described by stacked-disk scattering with radii of 1250 Å and 2.08  $\mu\text{m}$  [65, 66]. As a result, the GNP-surfactant aggregates take the form of stacked disk micelles with the GNPs decorated by surfactant layers. This picture is consistent with the work of Matarredona et al. on the stabilization of nanotube dispersions using SDBS [70]. They also postulated that the SDBS molecules wrapped round the external walls of nanotubes to give apparently cylindrical micelles. A recent review of the collective work on simulation studies by Lin et al. [53] also shows that the surfactant tails will distribute as much as possible on both graphene surfaces, giving “sandwich-like” assembled structures, although for certain surfactants e.g. SDBS some regions might still remain exposed to the aqueous phase.

For graphene-surfactant dispersions in water, there will be a dynamic equilibrium between surfactant molecules in the bulk phase, at the air-water interface and those adsorbed on graphene surfaces. Considering surfactants cover GNP surfaces uniformly, then surfactant adsorption could be described with a Langmuir isotherm, which is generally used to model the equilibrium adsorption from an ideal bulk solution to an ideal monolayer [46].

One way to estimate the surface concentration for the monolayer adsorption on graphenes is to consider the limiting surface excess ( $\Gamma$ ), which can be estimated reliably from aqueous surface tension data via the Gibbs equation (Eq 2). Here the Gibbs equation applied to the air – water interface has been used to gain insight into adsorption at the graphene aqueous interface, assuming adsorption at the two interfaces is essentially similar [23, 64]. (The assumption is that surface densities on GNP surfaces are similar to those at model air-water surfaces).

$$\Gamma = -\frac{1}{mRT} \frac{d\gamma}{\ln c} \quad (\text{Eq 2})$$

To estimate adsorption on graphene surfaces, data from the air-water surfaces were used as inputs to a Langmuir isotherm (Eq 3) for assessing limiting values of surface concentration of monolayers,  $\Gamma_m$  (mol m<sup>-2</sup>) and surface coverages ( $\theta$ ). Where  $C_1$  is the surfactant concentration in the bulk phase and  $a$  is a constant. Figure 9 summarizes the different adsorption isotherms for DC3Ph2 and TC3Ph3 surfactants. Aqueous surface tension data and values for  $C_1$ ,  $\Gamma_m$ ,  $\Gamma$  and  $\theta$  along with other physical parameters derived from surface tension data are given in **supplementary material** (Table S5).

$$\Gamma = \frac{\Gamma_m C_1}{C_1 + a} \quad (\text{Eq 3})$$

$$\theta = \frac{\Gamma}{\Gamma_m} \quad (\text{Eq 4})$$

Interestingly, the concentration needed to achieve the same surface coverage ( $\theta$ ) is significantly lower for TC3Ph3 ( $\theta = 1.00$ ,  $C_1 = 0.002$  M) than for the di-chain surfactant (DC3Ph2;  $\theta = 0.99$ ,  $C_1 = 0.007$  M). In other words, TC3Ph3 does not require as high a bulk concentration surfactant to attain full coverage ( $\theta = 1$ ). This order follows the graphene dispersion stabilities and electrical conductivities reported earlier in this paper.

#### 4. Conclusions

The aim of this study was to explore structural modifications of highly efficient surfactants for stabilizing graphene dispersions in hydrophilic natural rubber polymer matrices. This has been achieved by investigating a range of anionic surfactants which can be readily synthesized from commercially available precursors. A clear correlation was observed between the number of aromatic moieties of a given surfactant and its performance in stabilizing GNPs – NRL, as gauged by the electrical conductivity of the nanocomposites and  $\zeta$ -potentials of the particle surfaces. A similar trend in aromatic group numbers versus dispersion stability has been observed but for the aqueous graphene dispersions [34, 35].

These results have important implications for the rational design of graphene-compatible surfactants. The advantages are that this latex technique is relatively straightforward to carry out, and measured electrical conductivity enhancements can be used to screen target compounds expected to exhibit enhanced compatibility/interaction with graphene surfaces. Despite the fact that the final nanocomposite conductivities are notably lower than the extensive graphene/polymer nanocomposites in literature [1, 10, 26, 49], the enhancement is remarkably high given the

relatively low surfactant levels compared to other works using this latex technology approach [6, 9].

### **Acknowledgements**

The work funded under grants from the National Nanotechnology Directorate Division Research Grant; (NND Grantcode: 2014-0015-102-03), Kurita Water and Environment Foundation (Grant Code: 16P003), and the Fundamental Research Grant Scheme (FRGS; Grant code: 2015-0155-101-02). This project was supported by JSPS [KAKENHI, Grant-in-Aid for Young Scientists (A), No. 23685034], and Leading Research Organizations (RCUK [through EPSRC EP/I018301/1], ANR [13-G8ME-0003]) under the G8 Research Councils Initiative for Multi-lateral Research Funding— G8-2012. The authors thank the Science and Technology Facilities Council for allocation of beam time, travel and consumables (experiment number RB1710004). This work benefited from the use of the SasView application, originally developed under NSF Award DMR-0520547. SasView also contains code developed with funding from the EU Horizon 2020 programme under the SINE2020 project Grant No 654000.

### **Appendix A. Supplementary Material**

Additional details of surfactant characterization, aqueous surface tensions and SANS data at various concentrations

## References

1. (a) H. Kim, A. A. Abdala, C. W. Macosko, Graphene/Polymer Nanocomposites, *Macromolecules* 43 (2010) 6515-6530, <https://doi.org/10.1021/ma100572e>. (b) T. A. Saleh, V.K. Gupta, *Nanomaterials and Polymer Membranes: Synthesis, Characterizations, and Applications*, 1<sup>st</sup> ed: Elsevier, London, 2016
2. J. Texter, Graphene Dispersions, *Curr. Opin. Colloid Interface Sci* 19 (2014) 163-174, <https://doi.org/10.1016/j.cocis.2014.04.004>
3. M. Lotya, Y. Hernandez, P. J. King, R. J. Smith, V. Nicolosi, L. S. Karlsson, F. M. Blighe, S. De, Z. Wang, I. T. McGovern, G. S. Duesberg, J. N. Coleman, Liquid Phase Production of Graphene by Exfoliation of Graphite in Surfactant/Water Solutions, *J. Am. Chem. Soc* 131 (2009) 3611-3620, <https://doi.org/10.1021/ja807449u>
4. A. B. Suriani, M. D. Nurhafizah, A. Mohamed, I. Zainol, A. K. Masrom, A Facile One-Step Method for Graphene Oxide/Natural Rubber Latex Nanocomposite Production for Supercapacitor Applications, *Mater. Lett* 161 (2015) 665-668, <https://doi.org/10.1016/j.matlet.2015.09.050>
5. A. Mohamed, A. K. Anas, S. A. Bakar, T. Ardyani, W. M. W. Zin., S. Ibrahim, M. Sagisaka, P. Brown, J. Eastoe, Enhanced Dispersion of Multiwall Carbon Nanotubes in Natural Rubber Latex Nanocomposites by Surfactants Bearing Phenyl Groups, *J. Colloid Interface Sci* 455 (2015) 179-187, <https://doi.org/10.1016/j.jcis.2015.05.054>
6. C. F. Matos, F. Galembeck, A. J. G. Zarbin, Multifunctional and Environmentally Friendly Nanocomposites between Natural Rubber and Graphene or Graphene Oxide, *Carbon* 78 (2014) 469-479, <https://doi.org/10.1016/j.carbon.2014.07.028>

7. O. Regev, P. N. B. ElKati, J. Loos, C. E. Koning, Preparation of Conductive Nanotube-Polymer Composites using Latex Technology, *Adv. Mater* 16 (2004) 248-251, <https://doi.org/10.1002/adma.200305728>
8. J. Yu, K. Lu, E. Sourty, N. Grossiord, C. E. Koning, J. Loos, Characterization of Conductive Multiwall Carbon Nanotube/Polystyrene Composites Prepared by Latex Technology, *Carbon* 45 (2007) 2897-2903, <https://doi.org/10.1016/j.carbon.2007.10.005>
9. A. Mohamed, T. Ardyani, S. A. Bakar, P. Brown, M. Hollamby, M. Sagisaka, J. Eastoe, Graphene-philic Surfactants for Nanocomposites in Latex Technology, *Adv. Colloid Interface Sci* 230 (2016) 54-69, <https://doi.org/10.1016/j.cis.2016.01.003>
10. E. E. Tkalya, M. Ghislandi, G. de With, C. E. Koning, The Use of Surfactants for Dispersing Carbon Nanotubes and Graphene to Make Conductive Nanocomposites, *Curr. Opin. Colloid Interface Sci* 17 (2012) 225-232, <https://doi.org/10.1016/j.cocis.2012.03.001>
11. S. Glanzer, A. F. Sax, Carbon Nanotubes Dressed by Aromatic Molecules, *Mol. Phys* 111 (2013) 2427-2438, <https://doi.org/10.1080/00268976.2013.831499>
12. A. Mohamed, A. K. Anas, S. A. Bakar, A. A. Aziz, M. Sagisaka, P. Brown, J. Eastoe, A. Kamari, N. Hashim, I. M. Isa, Preparation of Multiwall Carbon Nanotubes (MWCNTs) Stabilised by Highly Branched Hydrocarbon Surfactants and Dispersed in Natural Rubber Latex Nanocomposites, *Colloid Polym. Sci* 292 (2014) 3013-3023, <https://doi.org/10.1007/s00396-014-3354-1>
13. W. Pichayakorn, J. Suksaeree, P. Boonme, W. Taweepreda, G. C. Ritthidej, Preparation of Deproteinized Natural Rubber Latex and Properties of Films Formed by Itself and Several Adhesive Polymer Blends, *Ind. Eng. Chem. Res* 51 (2012) 13393-13404, <https://doi.org/10.1021/ie301985y>

14. T.-M Wu, E.-C. Chen, Preparation and Characterization of Conductive Carbon Nanotube-Polystyrene Nanocomposites using Latex Technology, *Compos. Sci. Technol* 68 (2008) 2254-2259, <https://doi.org/10.1016/j.compscitech.2008.04.010>
15. R. Verdejo, M. M. Bernal, L. J. Romasanta,; M. A. Lopez-Manchado, Graphene Filled Polymer Nanocomposites, *J. Mater. Chem* 21 (2011) 3301-3310, <https://doi.org/10.1039/C0JM02708A>
16. D. G. Papageorgiou, I. A. Kinloch, R. J. Young, Graphene/Elastomer Nanocomposites, *Carbon* 95 (2015) 460-484, <https://doi.org/10.1016/j.carbon.2015.08.055>
17. H. Pang, L. Xu, D.-X. Yan, Z.-M. Li, Conductive Polymer Composites with Segregated Structures, *Prog. Polym. Sci* 39 (2014) 1908-1933, <https://doi.org/10.1016/j.progpolymsci.2014.07.007>
18. S. Kirkpatrick, Percolation and Conduction, *Rev. Mod. Phys* 45 (1973) 574, <https://doi.org/10.1103/RevModPhys.45.574>
19. N. Grossiord, M.-C. Hermant, E. Tkalya, Electrically Conductive Polymer-Graphene Composites Prepared Using Latex Technology, In *Polymer-Graphene Nanocomposites*, V. Mittal, Ed. The Royal Society of Chemistry: Dorchester, UK, 2012; Chapter 3, pp 66-85.
20. J. C. Grunlan, A. R. Mehrabi, M. V. Bannan, J. L. Bahr, Water-Based Single-Walled-Nanotube-Filled Polymer Composite with an Exceptionally Low Percolation Threshold, *Adv. Mater* 16 (2004) 150-153, <https://doi.org/10.1002/adma.200305409>
21. M. Ghislandi, E. Tkalya, S. Schillinger, C. E. Koning, G. de With, High Performance Graphene- and MWCNTs-based PS/PPO Composites Obtained via Organic Solvent Dispersion, *Compos. Sci. Technol* 80 (2013) 16-22, <https://doi.org/10.1016/j.compscitech.2013.03.006>

22. N. R. Biswal, S. Paria, Effect of Electrolyte Solutions on the Adsorption of Surfactants at PTFE-Water Interface, *Ind. Eng. Chem. Res* 49 (2010) 7060-7067, <https://doi.org/10.1021/ie100812k>
23. V. Sa, K. G. Kornev, Analysis of Stability of Nanotube Dispersions using Surface Tension Isotherms, *Langmuir* 27 (2011) 13451-13460, <https://doi.org/10.1021/la2028466>
24. S. Wang, M. Yi, Z. Shen, The Effect of Surfactants and Their Concentration on the Liquid Exfoliation of Graphene, *RSC Adv* 6 (2016) 56705-56710, <https://doi.org/10.1039/C6RA10933K>
25. K. M. F. Shahil, A. A. Balandin, Graphene-Multilayer Graphene Nanocomposites as Highly Efficient Thermal Interface Materials, *Nano Lett* 12 (2012) 861-867, <https://doi.org/10.1021/nl203906r>
26. E. Tkalya, M. Ghislandi, A. Alekseev, C. Koning, J. Loos, Latex-based Concept for the Preparation of Graphene-based Polymer Nanocomposites, *J. Mater. Chem* 20 (2010) 3035-3039, <https://doi.org/10.1039/B922604D>
27. Y. V. Syurik, M. G. Ghislandi, E. E. Tkalya, G. Paterson, D. McGrouther, O. A. Ageev, J. Loos, Graphene Network Organisation in Conductive Polymer Composites, *Macromol. Chem. Phys*, 213 (2012) 1251-1258, <https://doi.org/10.1002/macp.201200116>
28. H. Baniasadi, A Ramazani, S. Mashayekhan, F. Ghaderinezhad, Preparation of Conductive Polyaniline/Graphene Nanocomposites via In Situ Emulsion Polymerization and Product Characterization, *Synth. Met* 196 (2014) 199-205, <https://doi.org/10.1016/j.synthmet.2014.08.007>
29. J. S. Kim, J. H. Yun, I. Kim, S. E. Shim, Electrical Properties of Graphene/SBR Nanocomposite Prepared by Latex Heterocoagulation Process at Room Temperature, *J. Ind. Eng. Chem* 17 (2011) 325-330, <https://doi.org/10.1016/j.jiec.2011.02.034>



30. M. Ghislandi, E. Tkalya, A. Alekseev, C. Koning, G. de With, Electrical Conductive Behavior of Polymer Composites Prepared with Aqueous Graphene Dispersions, *Applied Materials Today* 1 (2015) 88-94, <https://doi.org/10.1016/j.apmt.2015.11.001>
31. D. Lin, B. Xing, Adsorption of Phenolic Compounds by Carbon Nanotubes: Role of Aromaticity and Substitution of Hydroxyl Groups, *Environ. Sci. Technol* 42 (2008) 7254-7259, <https://doi.org/10.1021/es801297u>
32. A. Di Crescenzo, P. Di Profio, G. Siani, R. Zappacosta, A. Fontana, Optimizing the Interactions of Surfactants with Graphitic Surfaces and Clathrate Hydrates, *Langmuir* 32 (2016) 6559-6570, <https://doi.org/10.1021/acs.langmuir.6b01435>
33. M. Suttipong, N. R. Tummala, B. Kitiyanan, A. Striolo, Role of Surfactant Molecular Structure on Self-Assembly: Aqueous SDBS on Carbon Nanotubes, *J. Phys. Chem. C* 115 (2011) 17286-17296, <https://doi.org/10.1021/jp203247r>
34. S. Das, F. Irin,.; H. S. Tanvir Ahmed, A. B. Cortinas, A. S. Wajid, D. Parviz, A. F. Jankowski, M. Kato, M. J. Green, Non-Covalent Functionalization of Pristine Few-Layer Graphene using Triphenylene Derivatives for Conductive Poly (Vinyl Alcohol) Composites, *Polymer* 53 (2012) 2485-2494, <https://doi.org/10.1016/j.polymer.2012.03.012>
35. D. Parviz, S. Das, H. S. T. Ahmed, F. Irin, S. Bhattacharia, M. J. Green, Dispersions of Non-Covalently Functionalized Graphene with Minimal Stabilizer, *ACS Nano* 6 (2012) 8857-8867, <https://doi.org/10.1021/nn302784m>
36. J. R. Potts, O. Shankar, L. Du, R. S. Ruoff, Processing-Morphology-Property Relationships and Composite Theory Analysis of Reduced Graphene Oxide/Natural Rubber Nanocomposites, *Macromolecules* 45 (2012) 6045-6055, <https://doi.org/10.1021/ma300706k>

37. J. R. Potts, O. Shankar, S. Murali, L. Du, R. S. Ruoff, Latex and Two-Roll Mill Processing of Thermally-Exfoliated Graphite Oxide/Natural Rubber Nanocomposites, *Compos. Sci. Technol* 74 (2013) 166-172, <https://doi.org/10.1016/j.compscitech.2012.11.008>
38. Y. Zhan, J. Wu, H. Xia, N. Yan, G. Fei, G. Yuan, Dispersion and Exfoliation of Graphene in Rubber by an Ultrasonically-Assisted Latex Mixing and In situ Reduction Process, *Macromol. Mater. Eng* 296 (2011) 590-602, <https://doi.org/10.1002/mame.201000358>
39. J. I. Paredes, S. Villar-Rodil, P. Solis-Fernandez, A. Martinez-Alonso, J. M. D. Tascon, Atomic Force and Scanning Tunneling Microscopy Imaging of Graphene Nanosheets Derived from Graphite Oxide, *Langmuir* 25 (2009) 5957-5968, <https://doi.org/10.1021/la804216z>
40. F. D. B. d. Sousa, C. H. Scuracchio, The Use of Atomic Force Microscopy as an Important Technique to Analyze the Dispersion of Nanometric Fillers and Morphology in Nanocomposites and Polymer Blends Based on Elastomers, *Polimeros* 24 (2014) 661-672, <http://dx.doi.org/10.1590/0104-1428.1648>
41. M. S. Dresselhaus, A. Jorio, M. Hofmann, G. Dresselhaus, R. Saito, Perspectives on Carbon Nanotubes and Graphene Raman Spectroscopy, *Nano Lett* 10 (2010) 751-758, <https://doi.org/10.1021/nl904286r>
42. A. C. Ferrari, J. C. Meyer, V. Scardaci, C. Casiraghi, M. Lazzeri, F. Mauri, S. Piscanec, D. Jiang, K. S. Novoselov, S. Roth, A. K. Geim, Raman Spectrum of Graphene and Graphene Layers, *Phys. Rev. Lett* 97 (2006) 187401(1-4), <https://doi.org/10.1103/PhysRevLett.97.187401>
43. T. L. Doane, C.-H. Chuang, R. J. Hill, C. Burda, Nanoparticle  $\zeta$ -Potentials, *Acc. Chem. Res* 45 (2012) 317-326, <https://doi.org/10.1021/ar200113c>

44. V. K. Paruchuri, A. V. Nguyen, J. D. Miller, Zeta-Potentials of Self-Assembled Surface Micelles of Ionic Surfactants Adsorbed at Hydrophobic Graphite Surfaces, *Colloids Surf., A* 250 (2004) 519-526, <https://doi.org/10.1016/j.colsurfa.2004.04.098>
45. R. J. Hunter, *Zeta Potential in Colloid Science: Principles and Applications*, 1<sup>st</sup> ed; Academic Press: London, 1986.
46. M. J. Rosen, *Surfactant and Interfacial Phenomena*, 3<sup>rd</sup> ed; John Wiley & Sons: New Jersey, 2004.
47. M. Lotya, P. J. King, U. Khan, S. De, J. N. Coleman, High-Concentration, Surfactant-Stabilized Graphene Dispersions, *ACS Nano* 4 (2010) 3155-3162, <https://doi.org/10.1021/nn1005304>
48. R. J. Smith, M. Lotya, J. N. Coleman, The Importance of Repulsive Potential Barriers for the Dispersion of Graphene using Surfactants, *New J. Phys* 12 (2010) 125008, <https://doi.org/10.1088/1367-2630/12/12/125008>
49. E. Tkalya, M. Ghislandi, R. Otten, M. Lotya, A. Alekseev, P. van der Schoot, J. Coleman, G. de With, C. Koning, Experimental and Theoretical Study of the Influence of the State of Dispersion of Graphene on the Percolation Threshold of Conductive Graphene/Polystyrene Nanocomposites, *ACS Appl. Mater. Interfaces* 6 (2014) 15113-15121, <https://doi.org/10.1021/am503238z>
50. P. A. Hassan, S. Rana, G. Verma, Making Sense of Brownian Motion: Colloid Characterization by Dynamic Light Scattering, *Langmuir* 31 (2014) 3-12, <https://doi.org/10.1021/la501789z>

51. J. Björk, F. Hanke, C.-A. Palma, P. Samori, M. Cecchini, M. Persson, Adsorption of Aromatic and Anti-Aromatic Systems on Graphene through  $\pi$ - $\pi$  Stacking, *J. Phys. Chem. Lett* 1 (2010) 3407-3412, <https://doi.org/10.1021/jz101360k>
52. S. Grimme, Do Special Noncovalent  $\pi$ - $\pi$  Stacking Interactions Really Exist? *Angew. Chem., Int. Ed* 47 (2008) 3430-3434, <https://doi.org/10.1002/anie.200705157>
53. S. Lin, C.-J. Shih, V. Sresht, A. G. Rajan, M. S. Strano, D. Blankshtein, Understanding the Colloidal Dispersion Stability of 1D and 2D Materials: Perspectives from Molecular Simulations and Theoretical Modeling, *Adv. Colloid Interface Sci* 244 (2016) 36-53, <https://doi.org/10.1016/j.cis.2016.07.007>
54. H. Wang, Dispersing Carbon Nanotubes using Surfactants, *Curr. Opin. Colloid Interface Sci* 14 (2009) 364-371, <https://doi.org/10.1016/j.cocis.2009.06.004>
55. L. A. Feigin, D. I. Svergun, *Structure Analysis by Small-Angle X-Ray and Neutron Scattering*, 1<sup>st</sup> ed: Springer: New York, 1987.
56. J. B. Hayter, J. Penfold, Determination of Micelle Structure and Charge by Neutron Small-Angle Scattering, *Colloid Polym. Sci* 261 (1983) 1022-1030, <https://doi.org/10.1007/BF01421709>
57. W. Zhou, M. F. Islam, H. Wang, D. L. Ho, A. G. Yodh, K. I. Winey, J. E. Fischer, Small Angle Neutron Scattering from Single-Wall Carbon Nanotube Suspensions: Evidence for Isolated Rigid Rods and Rod Networks, *Chem. Phys. Lett* 384 (2004) 185-189, <https://doi.org/10.1016/j.cplett.2003.11.106>
58. D. C. H. Cheng, E. Gulari, Micellization and Intermicellar Interactions in Aqueous Sodium Dodecyl Benzene Sulfonate Solutions, *J. Colloid Interface Sci* 90 (1982) 410-423, [https://doi.org/10.1016/0021-9797\(82\)90308-3](https://doi.org/10.1016/0021-9797(82)90308-3)

59. F. Palazzesi, M. Calvaresi, F. Zerbetto, A Molecular Dynamics Investigation of Structure and Dynamics of SDS and SDBS Micelles, *Soft Matter* 7 (2011) 9148-9156, <https://doi.org/10.1039/C1SM05708A>
60. P. Brown, C. Butts, R. Dyer, J. Eastoe, I. Grillo, F. Guittard, S. Rogers, R. Heenan, Anionic Surfactants and Surfactant Ionic Liquids with Quaternary Ammonium Counterions, *Langmuir* 27 (2011) 4563-4571, <https://doi.org/10.1021/la200387n>
61. A. Mohamed, K. Trickett, S. Y. Chin, S. Cummings, M. Sagisaka, L. Hudson, S. Nave, R. Dyer, S. E. Rogers, R. K. Heenan, J. Eastoe, Universal Surfactant for Water, Oils, and CO<sub>2</sub>, *Langmuir* 26 (2010) 13861-13866, <https://doi.org/10.1021/la102303q>
62. H. Wang, W. Zhou, D. L. Ho, K. I. Winey, J. E. Fischer, C. J. Glinka, E. K. Hobbie, Dispersing Single-Walled Carbon Nanotubes with Surfactants: A Small Angle Neutron Scattering Study, *Nano Lett* 4 (2004) 1789-1793, <https://doi.org/10.1021/nl048969z>
63. C. A. Silvera-Batista, K. J. Ziegler, Swelling the Hydrophobic Core of Surfactant-Suspended Single-Walled Carbon Nanotubes: A SANS Study, *Langmuir* 27 (2011) 11372-11380, <https://doi.org/10.1021/la202117p>
64. K. Yurekli, Mitchell, C. A.; Krishnamoorti, R., Small-Angle Neutron Scattering from Surfactant-Assisted Aqueous Dispersions of Carbon Nanotubes, *J. Am. Chem. Soc* 126 (2004) 9902-9903, <https://doi.org/10.1021/ja047451u>
65. M. Yoonessi, J. R. Gaier, Highly Conductive Multifunctional Graphene Polycarbonate Nanocomposites, *ACS Nano* 4 (2010) 7211-7220, <https://doi.org/10.1021/nn1019626>
66. E. M. Milner, N. T. Skipper, C. A. Howard, M. S. P. Shaffer, D. J. Buckley, K. A. Rahnejat, P. L. Cullen, R. K. Heenan, P. Lindner, R. Schweins, Structure and Morphology of Charged

Graphene Platelets in Solution by Small-Angle Neutron Scattering, *J. Am. Chem. Soc* 134 (2012) 8302-8305, <https://doi.org/10.1021/ja211869u>

67. L. Vaisman, H. D. Wagner, G. Marom, The Role of Surfactants in Dispersion of Carbon Nanotubes, *Adv. Colloid Interface Sci* 128-130 (2006) 37-46, <https://doi.org/10.1016/j.cis.2006.11.007>

68. A. B. Suriani, M. D. Nurhafizah, A. Mohamed, A. K. Masrom, V. Sahajwalla, R. K. Joshi, Highly Conductive Electrodes of Graphene Oxide/Natural Rubber Latex-Based Electrodes by using a Hyper-Branched Surfactant, *Mater. Des* 99 (2016) 174-181, <https://doi.org/10.1016/j.matdes.2016.03.067>

69. C. N. Rochette, J. J. Crassous, M. Drechsler, F. Gaboriaud, M. Eloy, B. de Gaudemaris, J. F. L. Duval, Shell Structure of Natural Rubber Particles: Evidence of Chemical Stratification by Electrokinetics and Cryo-TEM, *Langmuir* 29 (2013) 14655-14665, <https://doi.org/10.1021/la4036858>

70. O. Matarredona, H. Rhoads, Z. Li, J.H. Harwell, L. Balzano, D.E. Resasco, Dispersion of Single-Walled Carbon Nanotubes in Aqueous Solutions of the Anionic Surfactant NaDDBS, *J. Phys. Chem. B* 107 (2003) 13357-13367, <http://doi.org/10.1021/jp0365099>

## SUPPLEMENTARY MATERIAL

# **Rational Design of Aromatic Surfactants for Graphene/Natural Rubber Latex Nanocomposites with Enhanced Electrical Conductivity**

Azmi Mohamed<sup>1,2\*</sup>, Tretya Ardyani<sup>1</sup>, Suriani Abu Bakar<sup>2</sup>, Masanobu Sagisaka<sup>3</sup>, Yasushi Umetsu<sup>3</sup>, J.J. Hamon<sup>4</sup>, Bazura Abdul Rahim<sup>5</sup>, Siti Rahmah Esa<sup>5</sup>, Abdul Khalil Shawkataly<sup>6</sup>, Mohamad Hafiz Mamat<sup>7</sup>, Stephen King<sup>8</sup>, Julian Eastoe<sup>9</sup>

<sup>1</sup>Department of Chemistry, <sup>2</sup>Nanotechnology Research Centre, Faculty of Science and Mathematics, Universiti Pendidikan Sultan Idris, 35900 Tanjong Malim, Perak, Malaysia

<sup>3</sup>Department of Frontier Materials Chemistry, Graduate School of Science and Technology, Hirosaki University, Bunkyo-cho 3, Hirosaki, Aomori 036-8561, Japan

<sup>4</sup>School of Chemistry, Monash University, Clayton 3800, Australia.

<sup>5</sup>MIMOS Semiconductor Sdn Bhd (MSSB), Technology Park Malaysia, 57000 Bukit Jalil, Kuala Lumpur,

<sup>6</sup>School of Industrial Technology, Universiti Sains Malaysia, 11700 Gelugor, Penang, Malaysia

<sup>7</sup>NANO-SciTech Centre (NST), Institute of Science (IOS), Universiti Teknologi MARA (UiTM), 40450 Shah Alam, Selangor, Malaysia

<sup>8</sup>Rutherford Appleton Laboratory, ISIS Spallation Source, Chilton, Oxfordshire, OX110QT, United Kingdom

<sup>9</sup>School of Chemistry, University of Bristol, Cantock's Close, Bristol, BS8 1TS, United Kingdom

\*Corresponding author. Tel.: +601548117582; fax: +601548117296

E-mail address: azmi.mohamed@fsmf.upsi.edu.my

# <sup>1</sup>H NMR Spectroscopy

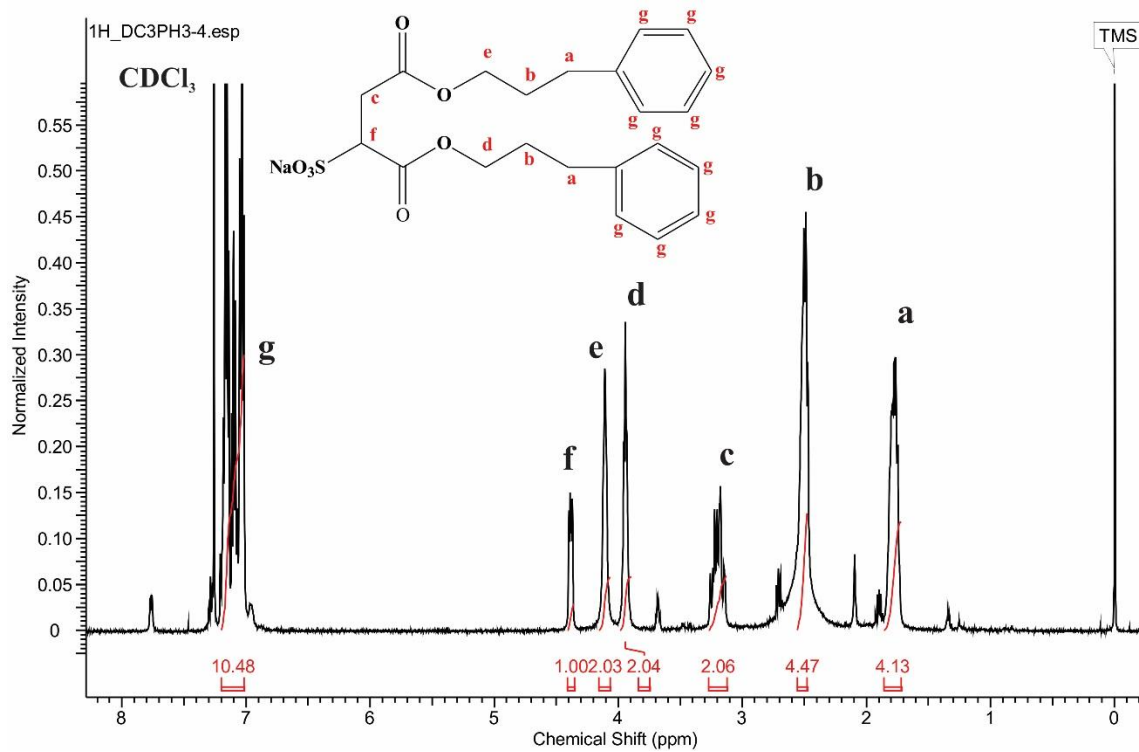


**Fig. S1.** <sup>1</sup>H NMR for DC3Ph2 surfactant. Solvent CDCl<sub>3</sub>.



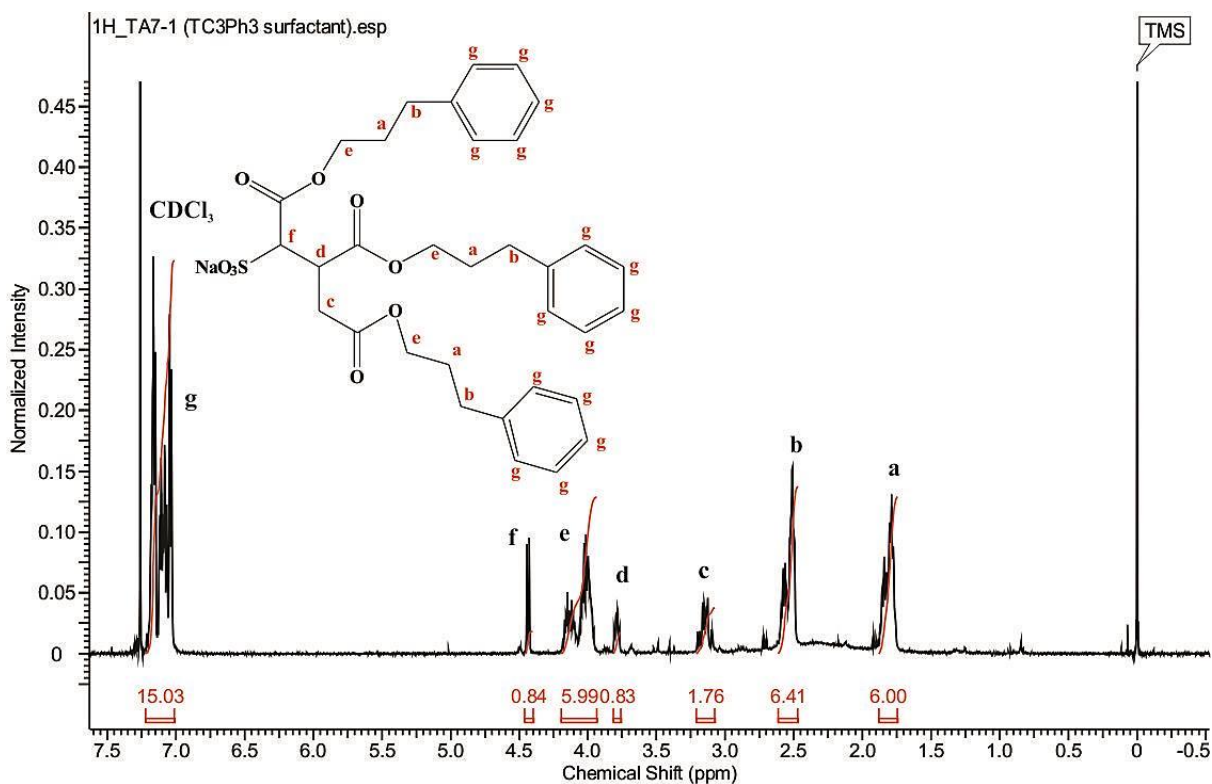


**Fig. S2.** <sup>1</sup>H NMR for TC3Ph3 surfactant. Solvent CDCl<sub>3</sub>.

**Table S1**

Comparison of theoretical and experimental <sup>1</sup>H NMR peak integrals for DC3Ph2 surfactant. Labels a to g represent the environment of each proton group in the surfactant.

Molecular fragment	Identified Proton	Chemical Shift	Relative NMR Integrals	
			Experimental	Theoretical
-C-CH <sub>2</sub> -C (aromatic)	a	1.75 – 1.85	4.13	4.00
-C-CH <sub>2</sub> -C-	b	2.47 – 2.50	4.47	4.00
O-CH <sub>2</sub> -C-	c	3.14 – 3.26	2.06	2.00
O-CH <sub>2</sub> -C-	d	3.89 – 3.95	2.04	2.00
S-C-CH <sub>2</sub> -C=O	e	4.06 – 4.11	2.03	2.00
C-CH*-SO <sub>3</sub> Na	f	4.37 – 4.40	1.00	1.00
-CH=CH Aromatic rings	g	7.02 – 7.19	10.48	10.00

$^1\text{H}$  NMR (500 MHz,  $\text{CDCl}_3$ , TMS), ( $\delta_{\text{H}}/\text{ppm}$ ): 1.75 – 1.85 (a, m, 4H), 2.47 – 2.50 (b, m, 4H), 3.14 – 3.26 (c, m, 2H), 3.89 – 3.95 (d, m, 2H), 4.06 – 4.11 (f, s, 1H), 7.02 – 7.19 (g, m, 15H)

**Table S2**

Comparison of theoretical and experimental  $^1\text{H}$  NMR peak integrals for TC3Ph3 surfactant. Labels a to g represent the environment of each proton group in the surfactant.

Molecular fragment	Identified Proton	Chemical Shift	Relative NMR Integrals	
			Experimental	Theoretical
C-CH <sub>2</sub> *-C=O	a	1.76 – 1.87	6.00	6.00
-C-CH <sub>2</sub> -C (aromatic)	b	2.47 – 2.60	6.41	6.00
-C-CH <sub>2</sub> -C=O	c	3.09 – 3.20	1.76	2.00
S-C-CH-C=O	d	3.77 – 3.81	0.83	1.00
O-CH <sub>2</sub> -C-	e	3.96 – 4.18	5.99	6.00
O <sub>3</sub> Na-S-CH-C-	f	4.43 – 4.44	0.84	1.00
-CH=CH Aromatic rings	g	7.03 – 7.21	15.03	15.00

$^1\text{H}$  NMR (500 MHz,  $\text{CDCl}_3$ , TMS), ( $\delta_{\text{H}}/\text{ppm}$ ): 1.76 – 1.87 (a, m, 6H), 2.47 – 2.60 (b, m, 6H), 3.09 – 3.20 (c, m, 2H), 3.77 – 3.81 (d, m, 1H), 3.96 – 4.18 (e, m, 6H), 4.43 – 4.44 (f, d, 1H,  $J = 5.0$  Hz), 7.03 – 7.21 (g, m, 15.0H)

## SANS data fitting

The scattering intensity  $I(Q)$  is proportional to the particle size and shape (form factor,  $P(Q)$ ) and interparticle interaction (structure factor,  $S(Q)$ ).

$$I(Q) \propto P(Q, R)S(Q) \quad (\text{Eq. S1})$$

Where  $R$  is the particle radius.

The raw SANS data were fitted to different models using the SASView interactive fitting program [1], which can be found online (<http://www.sasview.org/>).

Known parameters such as scattering length densities, dielectric constants and volume fractions can be set to constant values. Meanwhile, other unknown fit parameters obtained by allowing the program to refine them to achieve the optimized fit. The equations describing the form factors are described as follows.

## Spheres

This model provides the form factor,  $P(Q)$ , for a monodisperse spherical particle with uniform scattering length density. The form factor is normalized by the particle volume as following (Eq S2);

$$I(Q) = \frac{scale}{V} \cdot \left[ \frac{3V(\Delta\rho)(\sin(QR) - QR \cos(QR))}{(QR)^3} \right]^2 + bkg \quad (\text{Eq S2})$$

Where,  $scale$  is a factor used to put the intensity on an absolute scale,  $V$  is the volume of the scattering particle  $r$  is the radius of the sphere,  $bkg$  is the background level.

## Ellipsoid model

The form factor for oriented ellipsoids given by equations S3 to S5

$$P(\mathbf{q}, \alpha) = \frac{scale}{V} f^2(\mathbf{q}) + bkg \quad (\text{Eq S3})$$

$$f(\mathbf{q}) = \frac{3(\Delta\rho)V(\sin[qr(R_a, R_b, \alpha)] - qr \cos[qr(R_a, R_b, \alpha)])}{[qr(R_a, R_b, \alpha)]^3} \quad (\text{Eq S4})$$

$$r(R_a, R_b, \alpha) = [R_b^2 \sin^2 \alpha + R_a^2 \cos^2 \alpha]^{1/2} \quad (\text{Eq S5})$$

Where,  $\alpha$  is the angle between the axis of the ellipsoid and the  $q$ -vector,  $V$  is the volume of the ellipsoid,  $R_a$  is the radius along the rotational axis of the ellipsoid,  $R_b$  is the radius perpendicular to the rotational axis of the ellipsoid and  $\Delta\rho$  (contrast) is the scattering length density difference between the scattering particles and the solvent.

If the radius  $R_b > R_a$ , the object is an oblate ellipsoid (disk-like). If the  $R_b < R_a$ , the object is said to be prolate ellipsoid (rod-like). If both of the radii are equal, the object forms a spherical and is effectively described using sphere form factor above.

## Stacked-disk model

The form factor of stacked-disk (tactoids) model is given as;

$$I(q) = N \int_0^{\pi/2} [\Delta\rho_t(V_t f_t(q) - V_c f_c(q)) + \Delta\rho_c(V_c f_c(q))]^2 S(q) \sin \alpha d\alpha + bkg \quad (\text{Eq S6})$$

$$\langle f_t^2(q) \rangle_\infty = \int_0^{\pi/2} \left[ \left( \frac{\sin(q(d+h) \cos \alpha)}{q(d+h) \cos \alpha} \right) \left( \frac{2J_1(qR \sin \alpha)}{qR \sin \alpha} \right) \right]^2 \sin \alpha d\alpha \quad (\text{Eq S7})$$

$$\langle f_t^2(q) \rangle_\infty = \int_0^{\pi/2} \left[ \left( \frac{\sin(qh \cos \alpha)}{qh \cos \alpha} \right) \left( \frac{2J_1(qR \sin \alpha)}{qR \sin \alpha} \right) \right]^2 \sin \alpha d\alpha$$

$$S(q) = 1 + \frac{2}{n} \sum_{k=1}^n (n-k) \cos(kDq \cos \alpha) \exp[-k(q \cos \alpha)^2 \sigma_D / 2] \quad (\text{Eq S8})$$

Where, the parameters are  $N$  representing the number of disks per unit volume,  $\alpha$  is the angle between the axis of the disk,  $V_t$  and  $V_c$  respectively are the total volume and the core volume of a single disk,  $d$  is the thickness of the layer,  $2h$  is the core thickness,  $R$  is the radius of the disk ( $R_{disk}$ ). Scattering of a fully exfoliated monodisperse disks can be calculated by setting the total number of the disks stacked per tactoid ( $N$ ) equal to 1.

In this study, SANS data for a GNP dispersion stabilized by 0.01 M DC3Ph2 were fitted using a lamellar stack paracrystal model. The fit parameters were  $L$ , a mean layer thickness of  $N$  layers and  $D$ , layer separation. Meanwhile, the dispersion stabilized by 0.02 and 0.03 M surfactant respectively used the model for charge spherical and ellipsoidal form factor,  $P(Q)$  multiplied by a Hayter-Penfold charge repulsion [2] effective  $S(Q)$  for charged micelles. Scattering for dispersions

stabilized by TC3Ph3 at all surfactant concentrations was consistent with stacked 2D-material fragments [3, 4] and curves could be adequately fit by a stacked disk model.

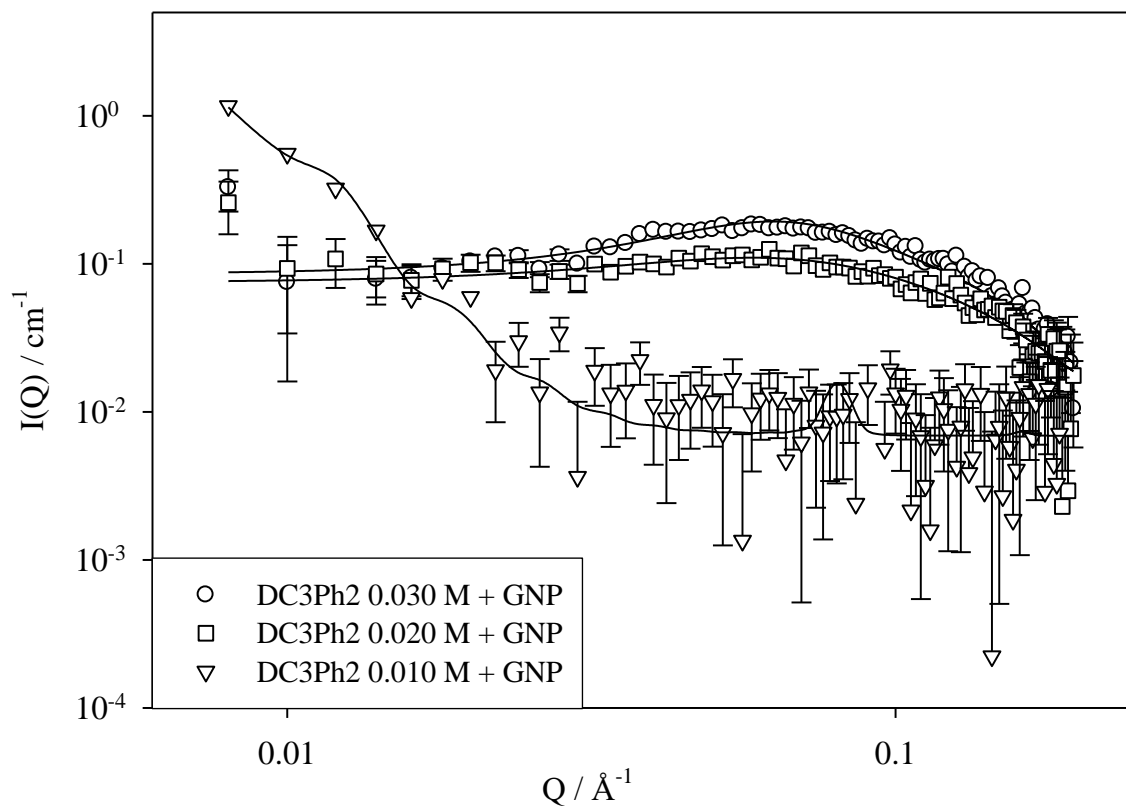


**Fig. S3.** SANS profiles of GNP-stabilized DC3Ph2 dispersions at various concentration

**Table S3**

Parameters fitted to SANS data from GNP-stabilized DC3Ph2 dispersions

Conc	Shape	$R_a$	$R_b$	$D$	$L$
(M)		( $\text{\AA} \pm 2$ )	( $\text{\AA} \pm 2$ )	( $\text{\AA} \pm 2$ )	( $\text{\AA} \pm 2$ )

0.01	Lamellar stack paracrystal	-	-	43.0	34.0
0.02	Spherical	17.0	-	-	-
0.03	Ellipsoidal	25.0	15.0	-	-

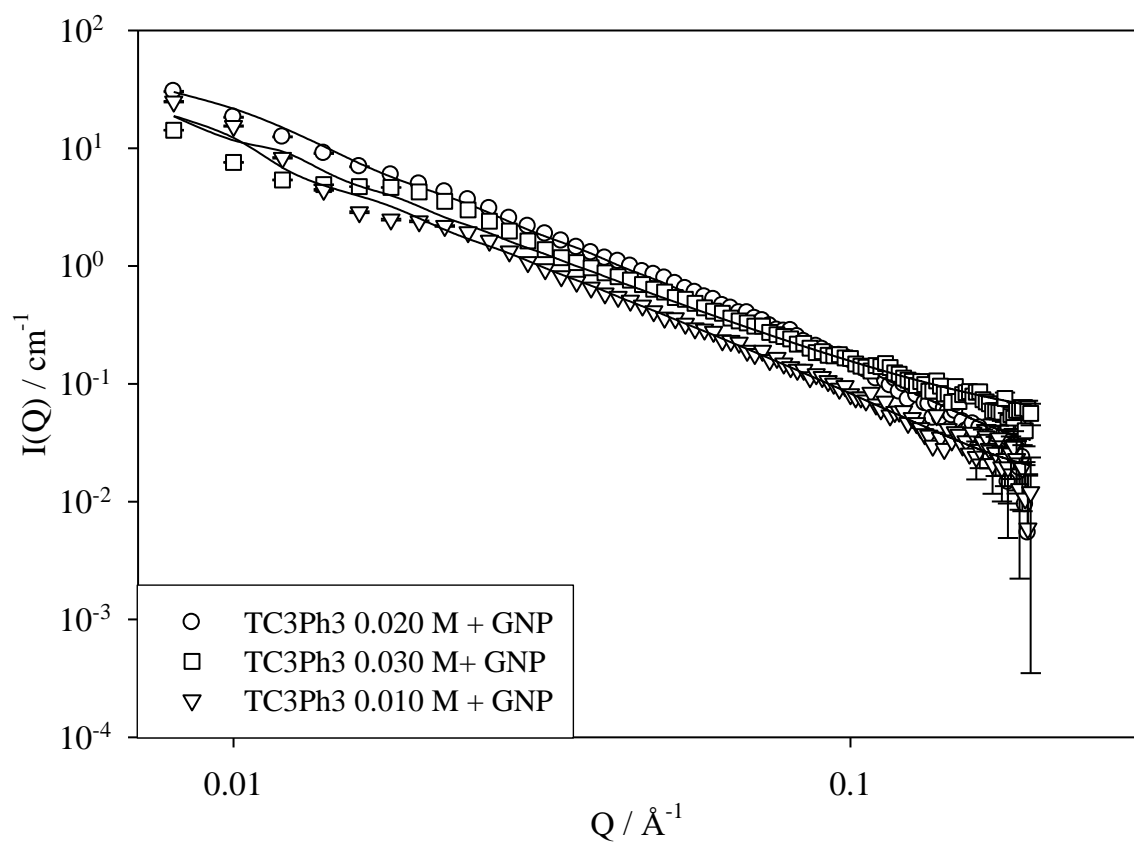


**Fig. S4.** SANS profiles for GNP-stabilized TC3Ph3 dispersions at various concentration

**Table S4**

Parameters fitted to SANS data of GNP-stabilized TC3Ph3 dispersion

Conc / M	Shape	R / Å ± 50
0.01	Stacked disk	200.0
0.02	Stacked disk	246.0
0.03	Stacked disk	286.0

**Guinier analysis**

The intensity,  $I(Q)$ , depends on contrast, particle numbers, particle volume and radius of gyration as shown in the following approximate equation, known as Guinier's law [5]:

$$I(Q) = \Delta\rho^2 N_p V_p^2 \exp(-Q^2 R_g^2 / 3) \quad (\text{Eq S9})$$

The  $R_g$  can be determined from the slope of the Guinier plot i.e.  $\ln I(Q)$  vs  $Q^2$  for any isometric particles. The radius of gyration ( $R_g$ ) can be conveniently used to characterize the size of a particle. It is the root mean square of the radius averaged over the volume of particle.<sup>5</sup> Theoretical radius value of each sample were estimated using Guinier plot and are given in Table S5 below.

**Table S5**

Radius obtained from Guinier approximation

Sample	Model	R / Å
SDBS	Sphere	22.0



---

DC3Ph2	Ellipsoid	17.0
TC3Ph3	Ellipsoid	21.0
SDBS + GNP	Sphere	22.0
DC3Ph2 + GNP	Ellipsoid	18.0
TC3Ph3 + GNP	Stacked Disk	215.0

---

### **Surface tension measurements**

Air-water (a/w) surface tensiometry was performed using a Wilhelmy tensiometer (CBVP-A3, Kyowa Interface Science) equipped with a platinum plate. All measurements were carried out at 25°C until the surface tension of the aqueous surfactant solutions reached constant (equilibrium) values. The critical micelle concentrations (cmc) of each surfactant solution were obtained from the intersection of the plots of the surface tension ( $\gamma$ ) versus  $\ln$  of concentration ( $\ln c$ ). The air-water surface tension measurements of DC3Ph2 and TC3Ph3 surfactants are shown in Figure S5.

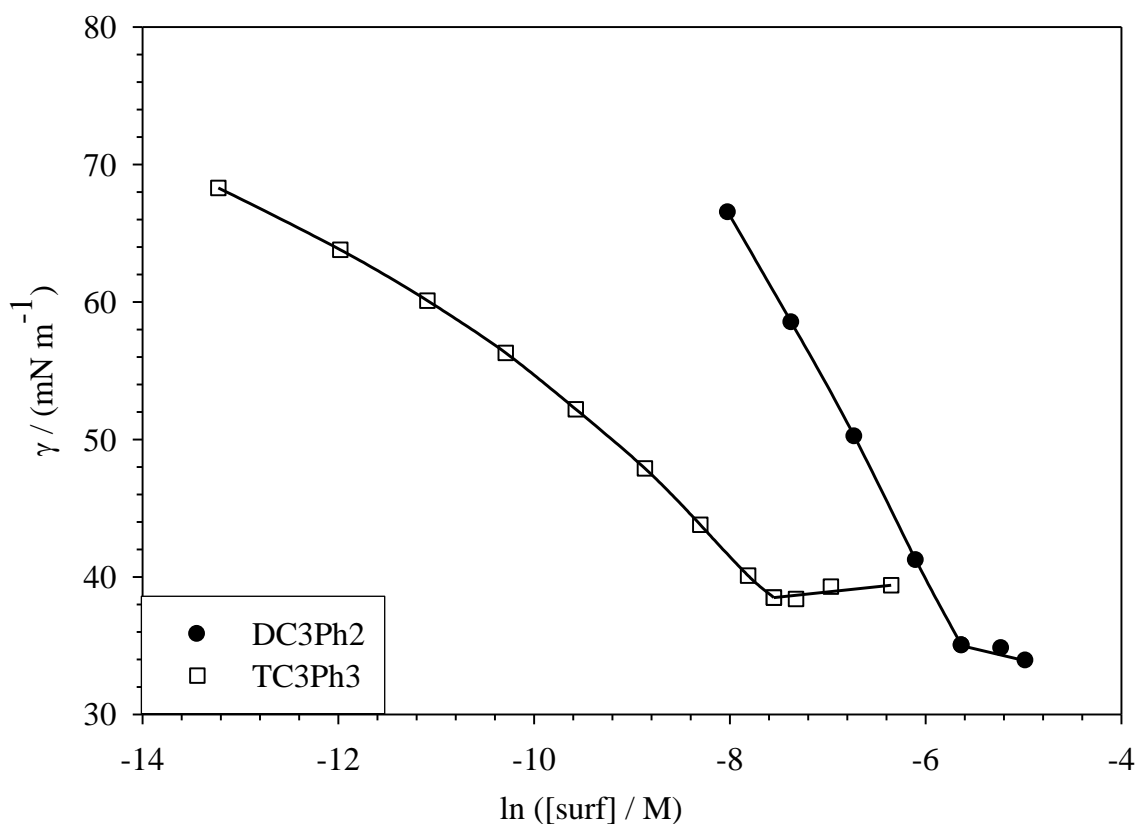


**Fig. S5.** Air – water surface tensions  $\gamma$  vs  $\ln(\text{concentration})$  for DC3Ph2 and TC3Ph3 surfactants at 25°C. Quadratic lines are fitted to pre-cmc data, with linear fits to post-cmc data.

As is well known in colloid science, changes in surfactant molecular structure has important implications for the physicochemical solution properties. Variations in length, branching, methylation and aromatization will tune the aqueous and interfacial properties [6-8]. Previous studies of phenyl-tipped of the aromatic analogues of Aerosol-OT (AOT) noted the of molecular volume of surfactant tail on addition of phenyls, in comparison to that of a simple linear alkyl chain [8]. It is instructive to compare the surface behaviour of the surfactants studied here with other AOT-analogues. Values for  $\Gamma_1$  were generated from the limiting headgroup areas at the

cmc ( $A_{\text{cmc}}$ ) value (Eq S10). The isotherm data and parameters derived from the surface tension measurements for the phenyl-tipped AOT-analogue surfactants are given in Table S6.

$$A_{\text{cmc}} = \frac{1}{\Gamma N_A} \quad (\text{Eq S10})$$

The surfactant surface excess ( $\Gamma$ ) obtained here is in similar range with those phenyl-tipped surfactants from literature (Table S7). An overall comparison across the series is that addition of the phenyls and carbon number of the linear chains both increase the area covered by surfactant molecules ( $\theta$  for the surfactant studied here,  $A_{\text{cmc}}$  for the phenyl-tipped series). It should be noted that the previous study did not determine the Langmuir isotherm so the  $\theta$  values cannot be directly compared those presented here, rather the areas occupied per surfactant molecule ( $A_{\text{cmc}}$ ) can be compared [9]. Despite these limitations, these observations represent the importance of aromatic groups in the surfactant chains to increase the surfactant molecular areas on graphene surfaces.

**Table S6**

Parameters derived from surface tension data and Langmuir isotherm plot

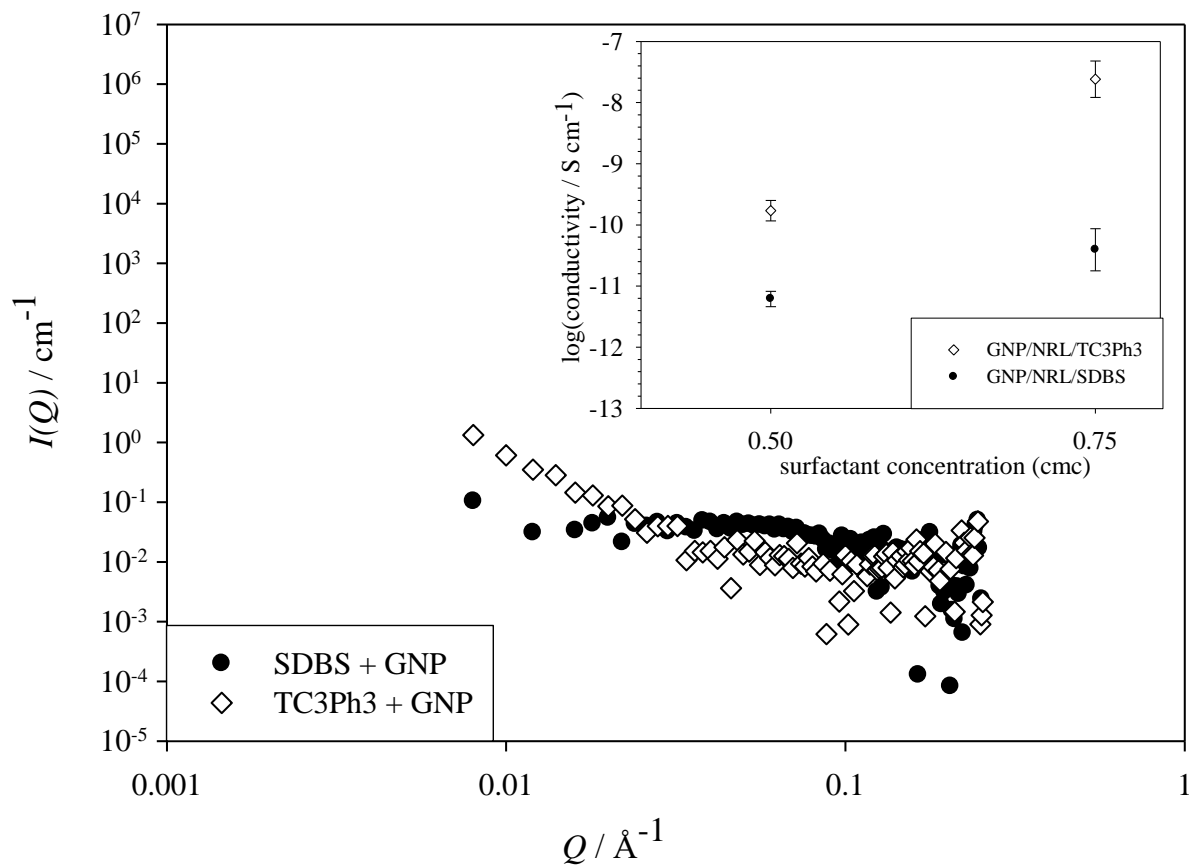
Surfactant	C <sub>mc</sub> (M)	C <sub>1</sub> (M) <sup>a</sup>	Γ (mol m <sup>-2</sup> )	Γ <sub>m</sub> (mol m <sup>-2</sup> )	θ
DC3Ph2	0.0036	0.007	3.016 x 10 <sup>-6</sup>	3.058 x 10 <sup>-6</sup>	0.99
TC3Ph3	0.0005	0.002	1.756 x 10 <sup>-6</sup>	1.750 x 10 <sup>-6</sup>	1.00

<sup>a</sup>Concentration at fully coverage surface.**Table S7**Parameters derived from surface tension data of the phenyl-tipped AOT-analogue surfactants<sup>a</sup>

Surfactant	C <sub>1</sub> (M)	A <sub>cmc</sub> / m <sup>2</sup>	Γ (mol m <sup>-2</sup> )
di-PhC4SS	0.0042	6.9 x 10 <sup>-19</sup>	2.4 x 10 <sup>-6</sup>
di-PhC5SS	0.0008	7.1 x 10 <sup>-19</sup>	2.3 x 10 <sup>-6</sup>
br-di-PhC3SS	0.0138	1.0x 10 <sup>-18</sup>	1.7 x 10 <sup>-6</sup>
br-di-PhC5SS	0.0017	9.8 x 10 <sup>-19</sup>	1.7 x 10 <sup>-6</sup>

<sup>a</sup>Data taken from ref [8]. br-coded surfactants are the isomer of the respective surfactants with difference on the chain branching. The surfactant chemical structure can be found in the noted reference.

## SANS profiles and electrical conductivity measurements of nanocomposites below cmc

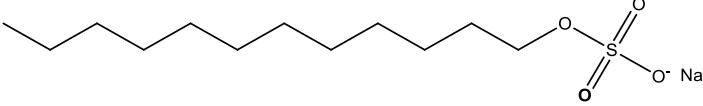
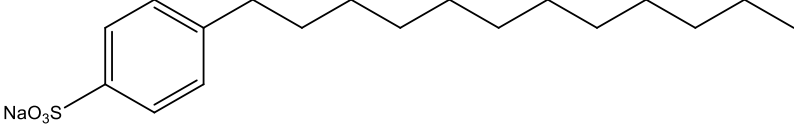
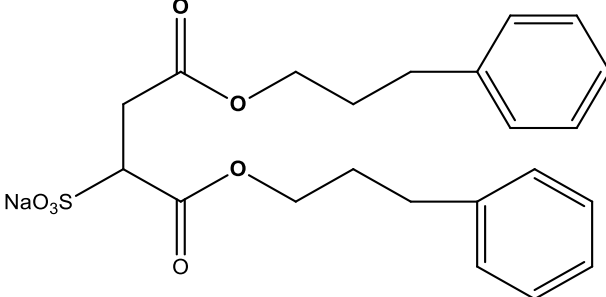
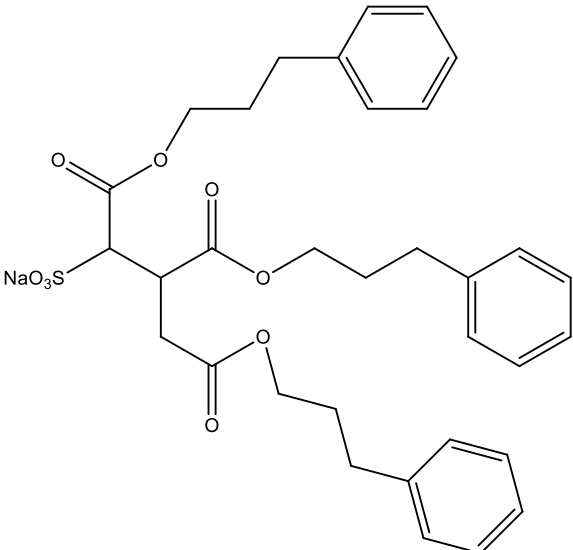


**Fig. S6.** SANS profiles of dispersions stabilized by SDBS and TC3Ph3 surfactant at concentrations below cmc. Inset shows and electrical conductivities of the corresponding nanocomposites.

## References

1. M. Doucet, et al. SasView Version 4.1.2, Zenodo, <http://doi.org/10.5281/zenodo.825675>
  2. J. B. Hayter, J. Penfold, Determination of Micelle Structure and Charge by Neutron Small-Angle Scattering, *Colloid Polym. Sci* 261 (1983) 1022-1030, <https://doi.org/10.1007/BF01421709>
  3. M. Yoonessi, J. R. Gaier, Highly Conductive Multifunctional Graphene Polycarbonate Nanocomposites, *ACS Nano* 4 (2010) 7211-7220, <https://doi.org/10.1021/nn1019626>
  4. E. M. Milner, N. T. Skipper, C. A. Howard, M. S. P. Shaffer, D. J. Buckley, K. A. Rahnejat, P. L. Cullen, R. K. Heenan, P. Lindner, R. Schweins, Structure and Morphology of Charged Graphene Platelets in Solution by Small-Angle Neutron Scattering, *J. Am. Chem. Soc* 134 (2012) 8302-8305, <https://doi.org/10.1021/ja211869u>
  5. L. A. Feigin, D. I. Svergun, Structure Analysis by Small-Angle X-Ray and Neutron Scattering, 1<sup>st</sup> ed: Springer: New York, 1987.
  6. S. Nave, J. Eastoe, J. Penfold, What Is So Special about Aerosol-OT? 1. Aqueous Systems, *Langmuir* 16 (2000) 8733-8740, <https://doi.org/10.1021/la000341q>
  7. S. Nave, J. Eastoe, R. K. Heenan, D. Steytler, I. Grillo, What Is So Special about Aerosol-OT? Part III - Glutaconate versus Sulfosuccinate Headgroups and Oil-Water Interfacial Tensions, *Langmuir* 18 (2002) 1505-1510, <https://doi.org/10.1021/la015564a>
  8. S. Nave, A. Paul, J. Eastoe, A. R. Pitt, R. K. Heenan, What Is So Special about Aerosol-OT? Part IV. Phenyl-Tipped Surfactants, *Langmuir* 21 (2005) 10021-10027, <https://doi.org/10.1021/la050767a>
- J. N. Israelachvili, D. J. Mitchell, B. W. Ninham, Theory of Self-Assembly of Hydrocarbon Amphiphiles into Micelles and Bilayers, *J. Chem. Soc., Faraday Trans. 2* 72 (1976) 1525-1568, <https://doi.org/10.1039/F29767201525> **Table 1**

Chemical structures of surfactants used in this work

Surfactant	Structure	Chemical Name
SDS		Sodium dodecylsulfate
SDBS		Sodium dodecylbenzenesulfonate
DC3Ph2		Sodium 1,4-dioxo-1,4-bis(3-phenylpropoxy)butane-2-sulfonate
TC3Ph3		Sodium 1,5-dioxo-1,5-bis(3-phenylpropoxy)-3-((3-phenylpropoxy)carbonyl)pentane-2-sulfonate

**Table 2**

Electrical conductivity of the GNP/NR-Latex nanocomposites stabilized by surfactants

Surfactant	cmc (M)	$\gamma_{cmc}$ (mN m <sup>-1</sup> )	Surfactant concentration (M)						
			0.004	0.008	0.012	0.015	0.020	0.024	0.032
			Electrical conductivity of nanocomposites (S cm <sup>-1</sup> )						
TC3Ph3	0.0005	38.9	$5.90 \times 10^{-6}$	$8.55 \times 10^{-6}$	$1.54 \times 10^{-5}$	$2.22 \times 10^{-5}$	$9.53 \times 10^{-6}$	$1.81 \times 10^{-6}$	$1.00 \times 10^{-6}$
DC3Ph2	0.0036	34.9	$8.82 \times 10^{-8}$	$3.42 \times 10^{-7}$	$3.12 \times 10^{-7}$	$3.39 \times 10^{-7}$	$6.56 \times 10^{-7}$	$9.19 \times 10^{-6}$	$9.36 \times 10^{-6}$
SDBS	0.0015 <sup>a</sup>	36.5 <sup>a</sup>	$5.61 \times 10^{-9}$	$4.75 \times 10^{-7}$	$7.03 \times 10^{-7}$	$1.76 \times 10^{-6}$	$3.42 \times 10^{-6}$	$3.55 \times 10^{-6}$	$3.04 \times 10^{-6}$
SDS	0.0080 <sup>b</sup>	34.7 <sup>b</sup>	$1.32 \times 10^{-9}$	$5.25 \times 10^{-9}$	$4.44 \times 10^{-9}$	$4.05 \times 10^{-9}$	$9.06 \times 10^{-9}$	$1.59 \times 10^{-8}$	$1.76 \times 10^{-8}$

<sup>a</sup>Data collected by Biswal and Paria [22]<sup>b</sup>Data collected by Sa and Kornev [23]



**Table 3**

$\zeta$ -potential data for graphene dispersions with different surfactants.

<b>Surfactant</b>	<b>Number of aromatic ring(s)</b>	<b><math>\zeta</math>-potential / mV</b>	<b>Electrical conductivity enhancement</b>
SDS	N/A	$-43 \pm 4$	$1.17 \times 10^6$
SDBS	1	$-40 \pm 8$	$2.36 \times 10^8$
DC3Ph2	2	$-69 \pm 7$	$6.21 \times 10^8$
TC3Ph3	3	$-95 \pm 6$	$1.47 \times 10^9$

**Table 4**Model fit parameters for the SANS Data<sup>a</sup>

Sample	Model	$R_{\text{sphere}} \pm 2 \text{ \AA}$	$R_a^b \pm 2 \text{ \AA}$	$R_b^c \pm 2 \text{ \AA}$	$R_{\text{disk}} \pm 50 \text{ \AA}$	$X \pm 0.2$
SDBS	Sphere	22.0	-	-	-	-
DC3Ph2	Ellipsoid	-	5.0	24.0	-	4.8
TC3Ph3	Ellipsoid	-	5.0	32.0	-	6.4
SDBS + GNP	Sphere	22.0	-	-	-	-
DC3Ph2 + GNP	Ellipsoid	-	25.0	15.0	-	0.6
TC3Ph3 + GNP	Stacked Disk	-	-	-	286.0	-
GNP	N/A	-	-	-	-	-

<sup>a</sup>[surf.] = 0.030 M except for GNP only. Charged micelles were fitted with interparticle structure factor  $S(Q)$  for Hayter-Penfold model. <sup>b</sup>Radius polar. <sup>c</sup>Radius equatorial.

## Figure Captions

**Fig. 1.** Electrical conductivities of the NRL matrices and GNP/NRL composites containing phenyl-functionalized surfactants. The error bars are given for three experimental measurements.

**Fig. 2.** Electrical conductivity enhancements with graphene/polymer nanocomposites. Characteristic error bars of three experimental measurements are shown for certain samples.

**Fig. 3.** FESEM images of GNP (a and a'), NRL (b and b'), GNP/NRL: without surfactant (c and c'), with SDS (d and d'), with SDBS (e and e'), with DC3Ph2 (f and f') and with TC3Ph3 (g and g').

**Fig. 4.** TEM micrographs of GNP/NRL/TC3Ph3 nanocomposites.

**Fig. 5.** AFM tapping mode images of GNP/NRL/TC3Ph3 surfactant composites [surf] = 0.016 M. (a) height image. (b) phase image.

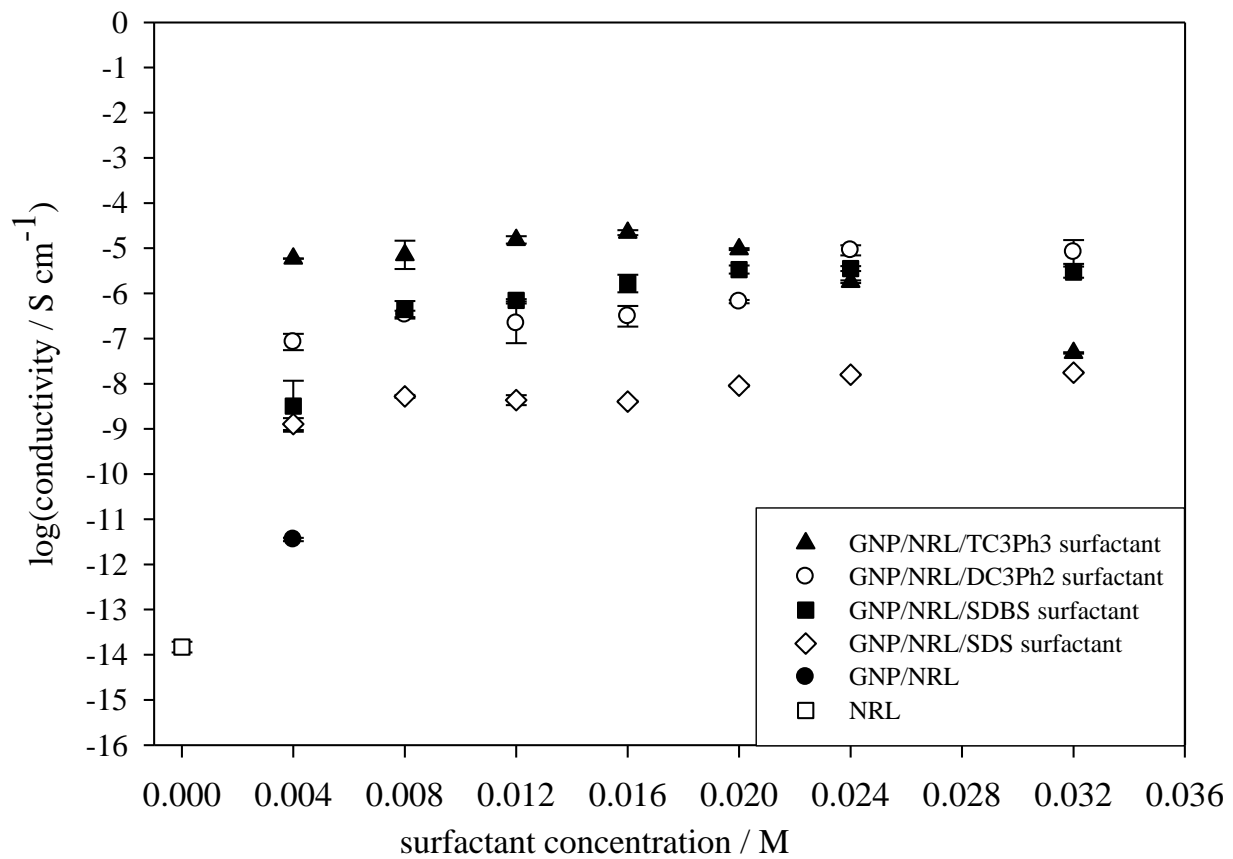
**Fig. 6.** Raman spectroscopy of graphene and nanocomposites. (a) GNP, (b) GNP/NRL, (c) GNP/NRL/SDS, (d) GNP/NRL/SDBS, (e) GNP/NRL/DC3Ph2, (f) GNP/NRL/TC3Ph3.

**Fig. 7.** SANS profiles for SDBS, DC3Ph2, TC3Ph3 surfactants solutions and GNP dispersions. [Surfactant] = 0.03 M and T = 25°C. Lines are model fits for charged spherical and ellipsoidal micelles (with and effective Hayter-Penfold  $S(Q)$ ), or stacked disk model (TC3Ph3 + GNP only). Characteristic error bars are shown for the lowest intensity samples.

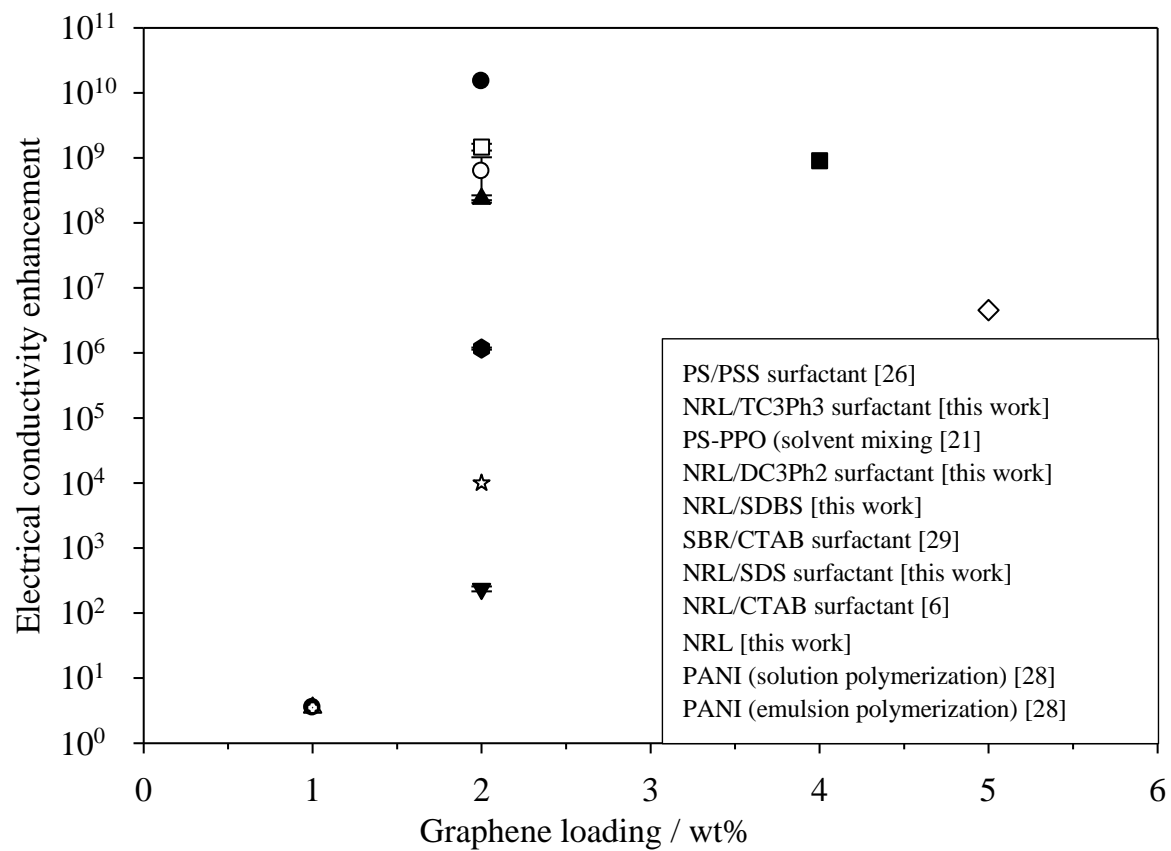
**Fig. 8.** Schematic of surfactant self-assembly in GNP/NRL systems

**Fig. 9.** Langmuir adsorption isotherms for (a) DC3Ph2 (b) TC3Ph3 surfactants. Characteristic error bars are shown to represent uncertainties for three experimental measurements.

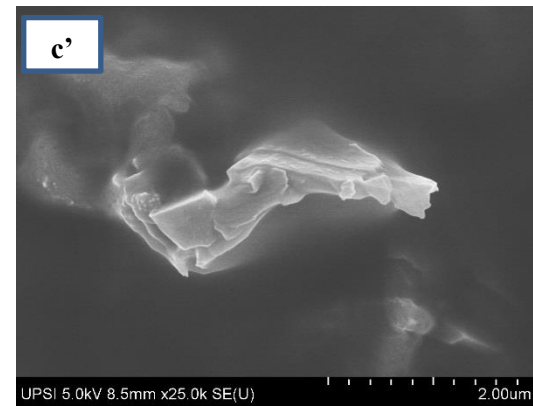
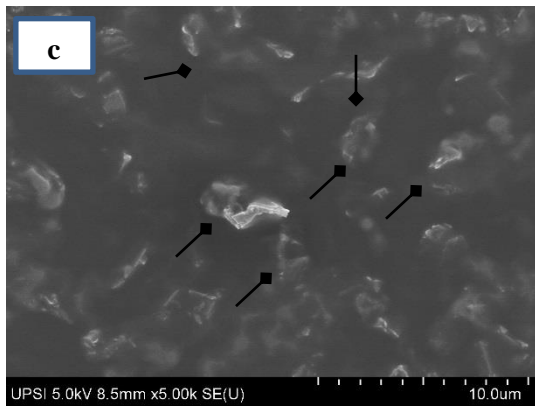
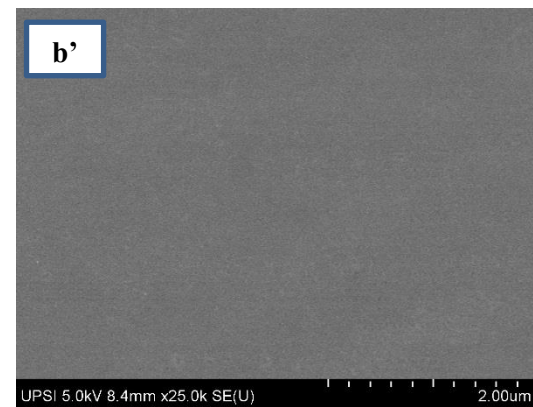
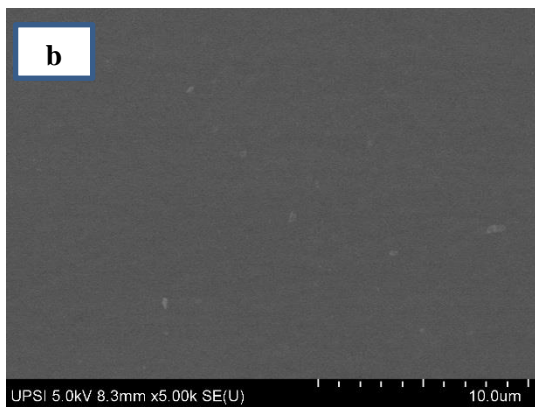
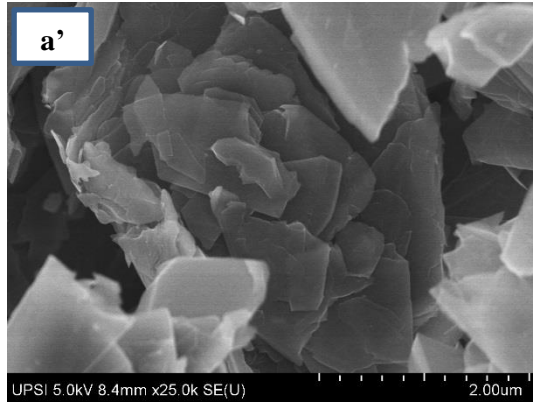
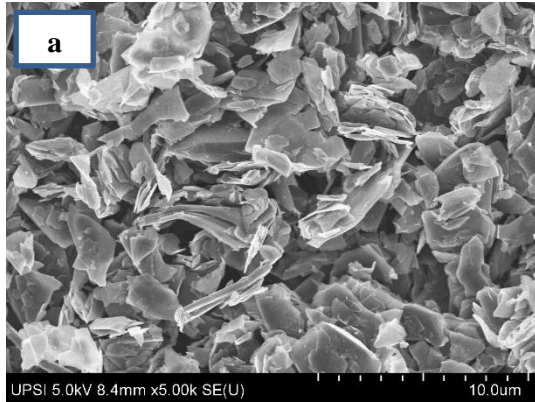
Fig. 1



**Fig. 2**



**Fig. 3**



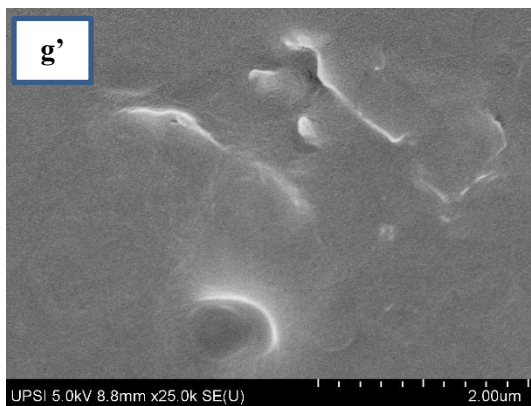
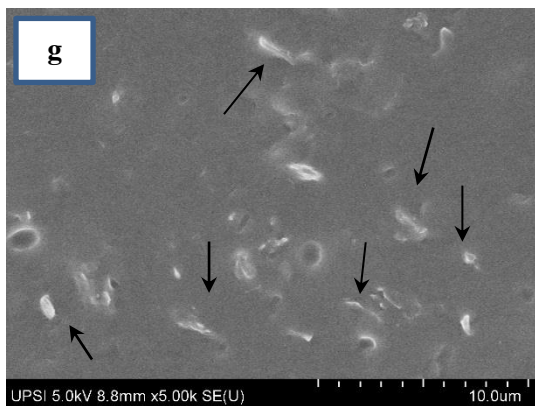
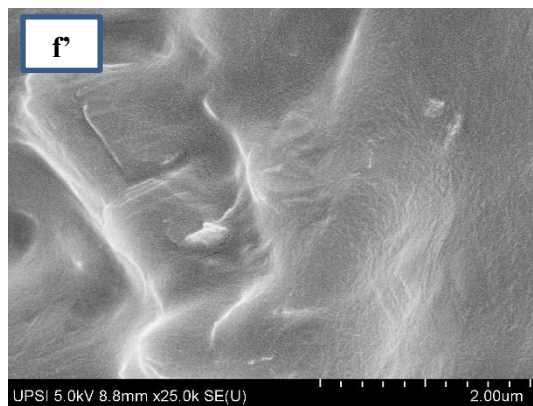
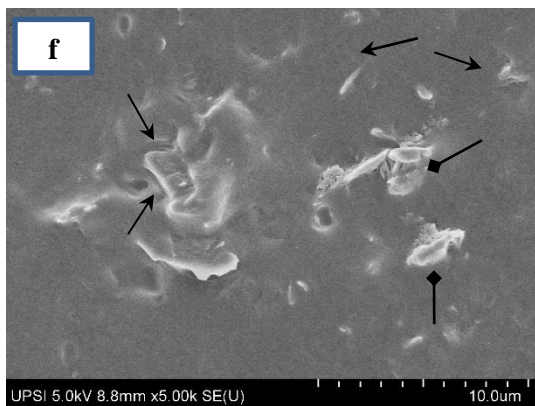
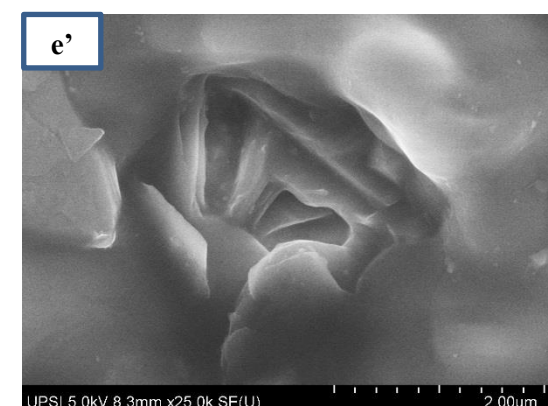
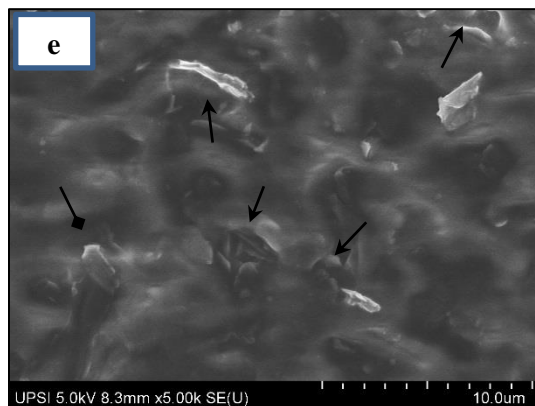
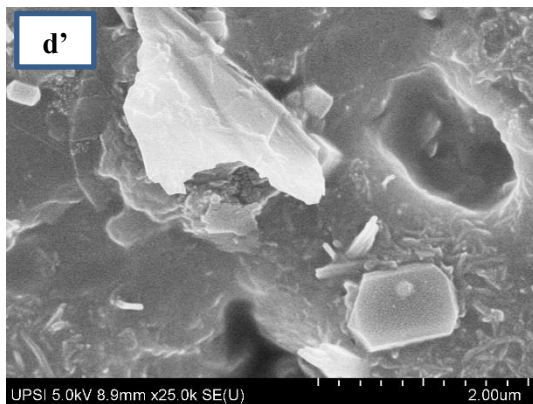
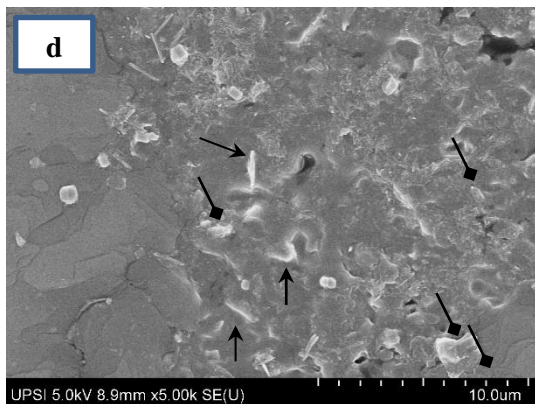


**Fig. 4**

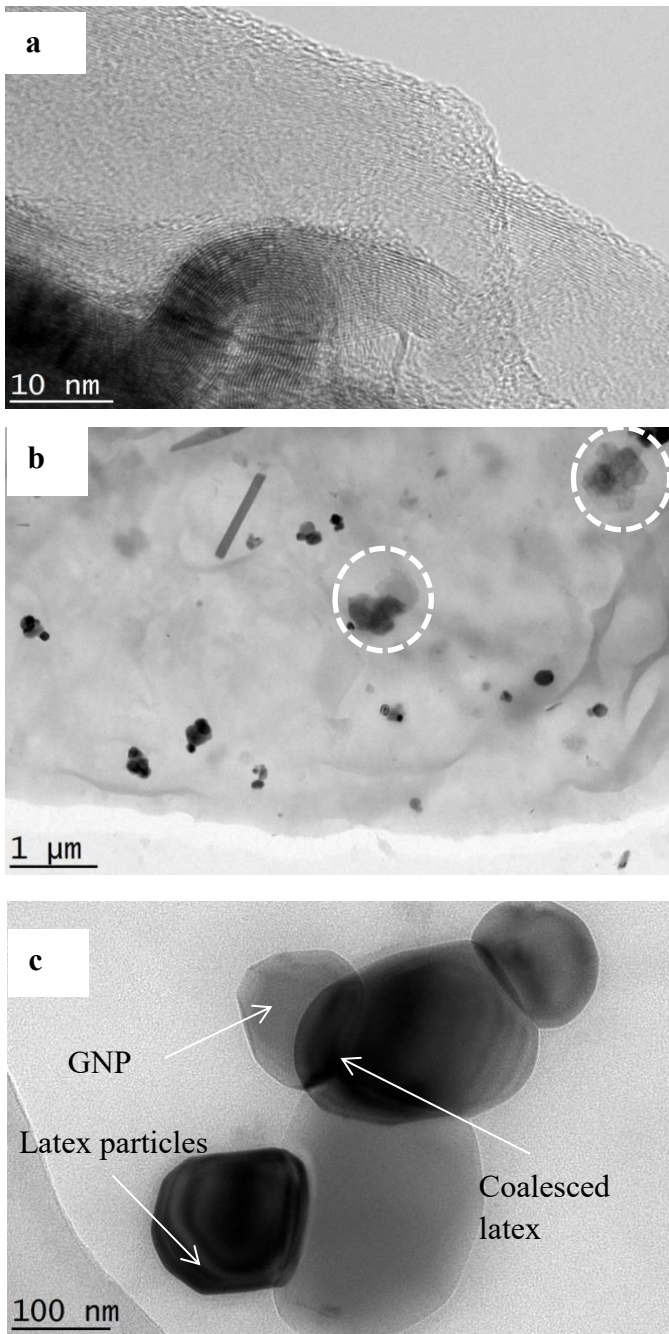
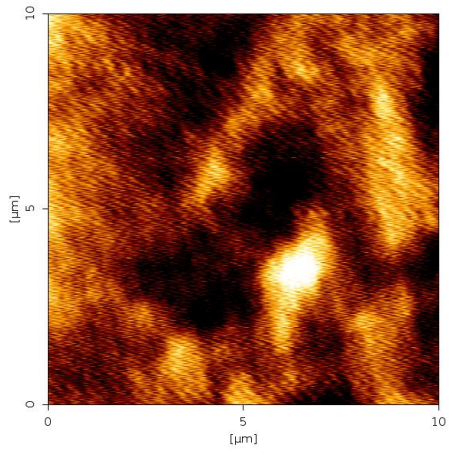
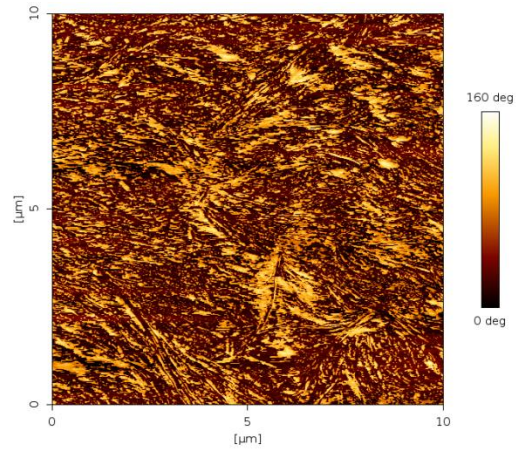




**Fig. 5**



(a)



(b)

**Fig. 6**

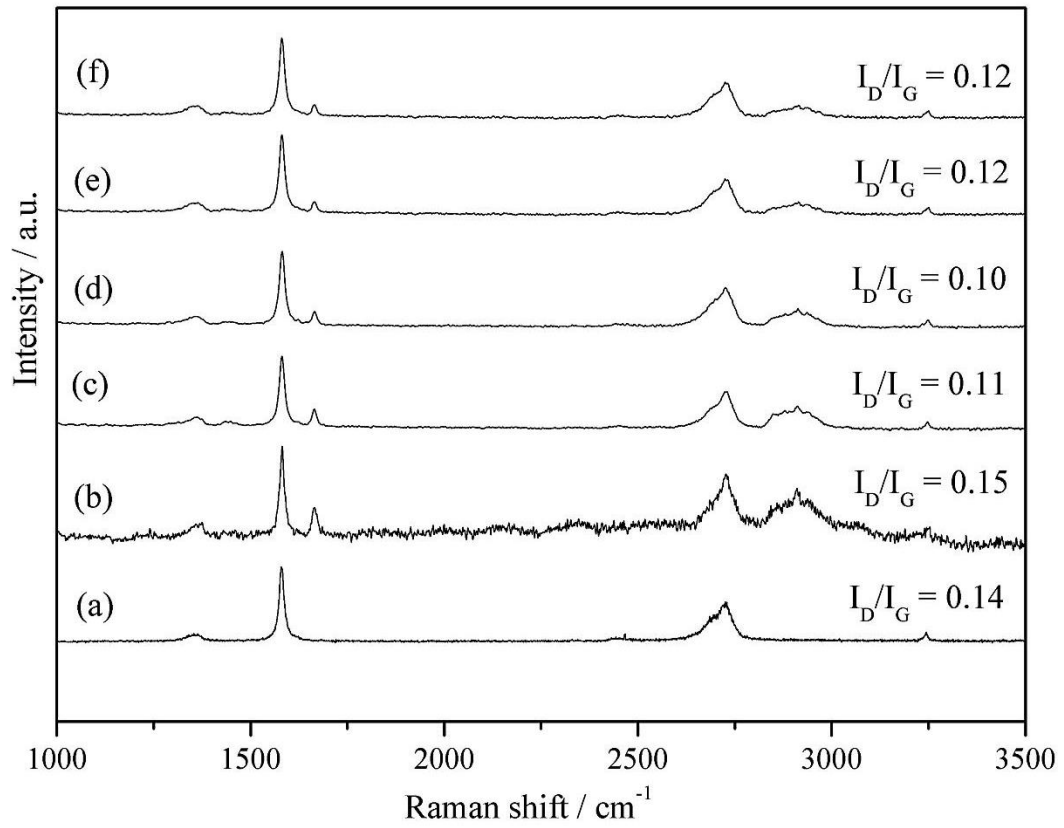


**Fig. 7**

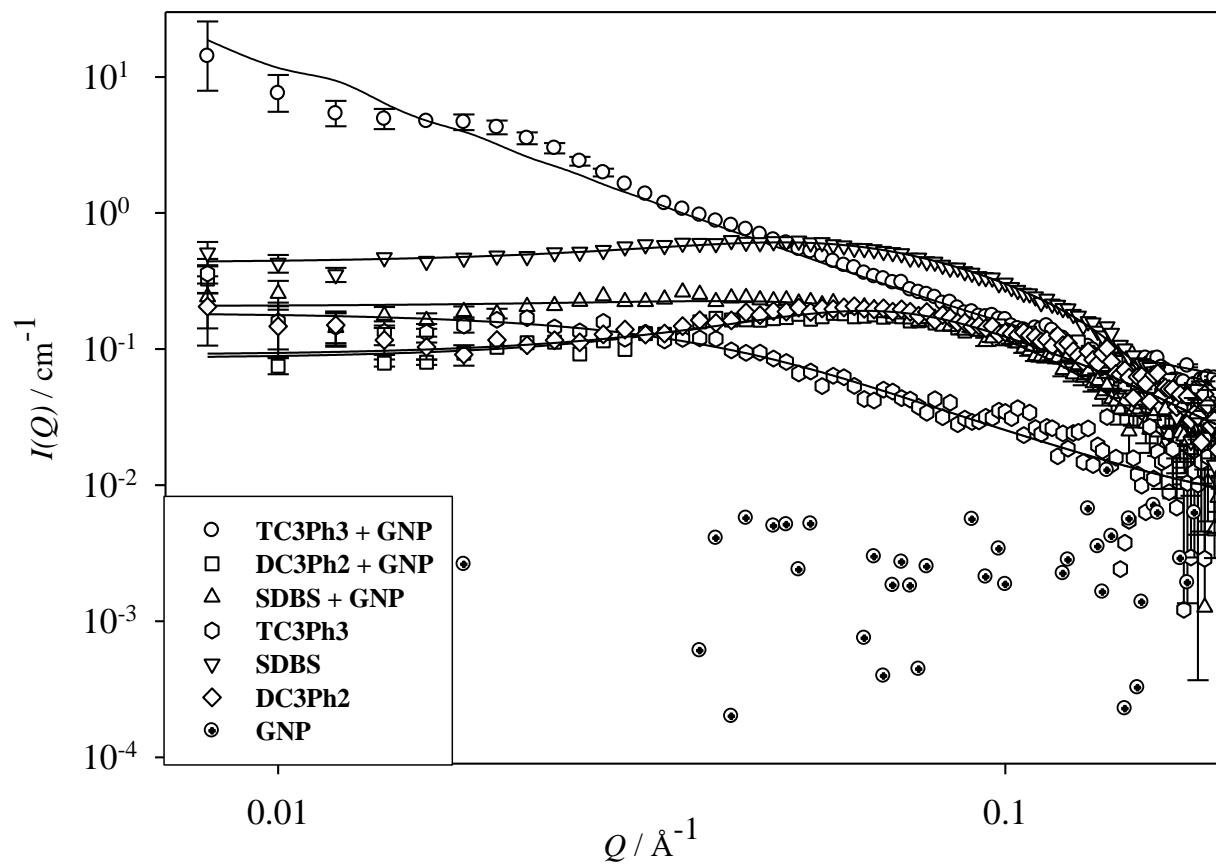
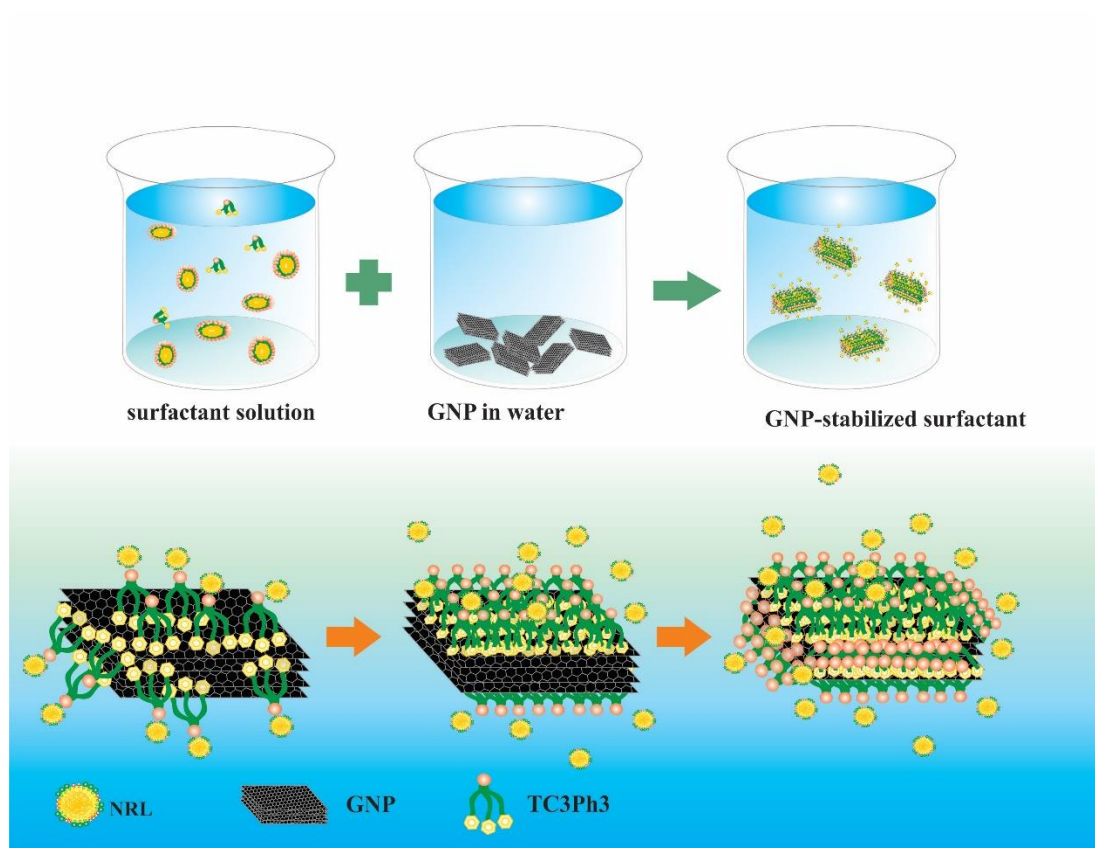
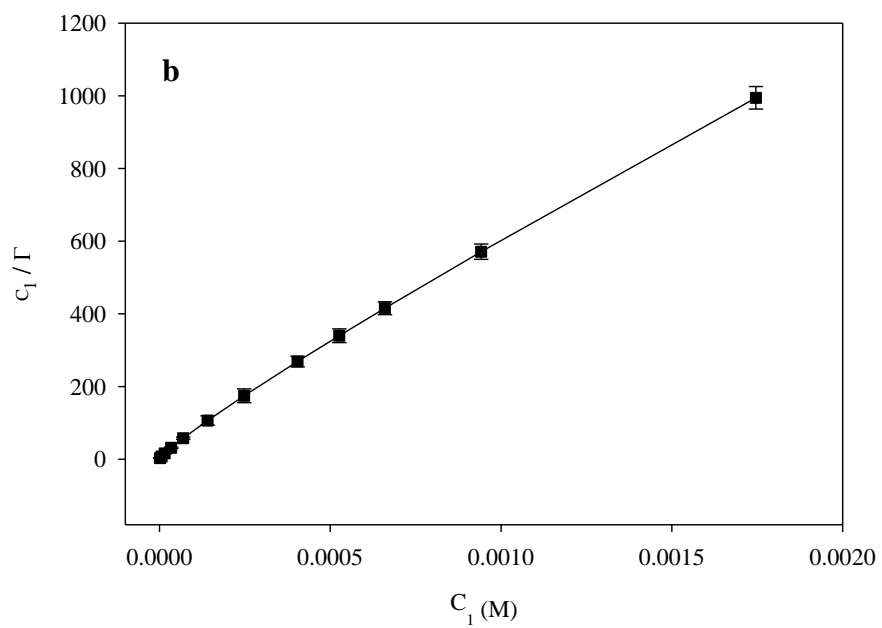
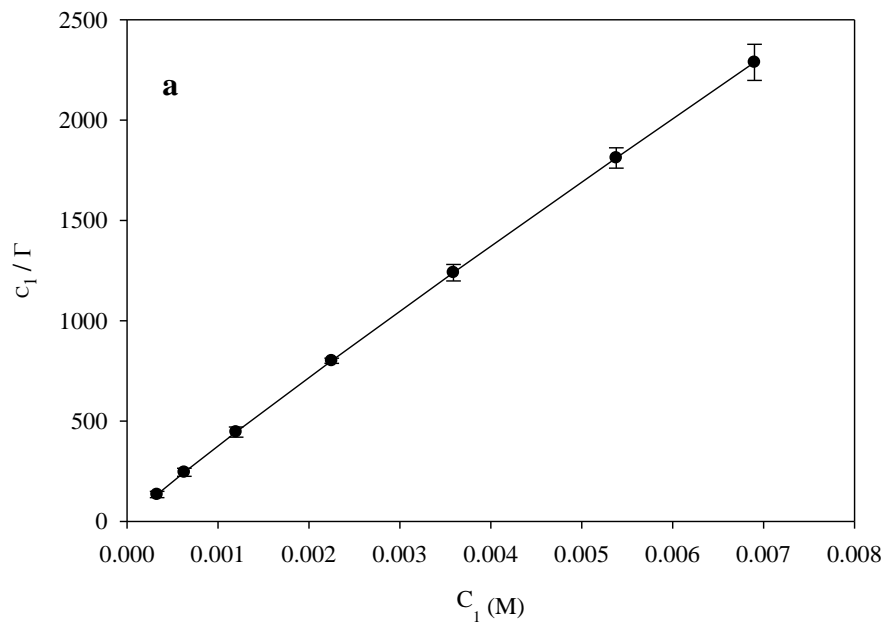


Fig. 8



**Fig. 9**



9.